Andrea Cäcilia Schuster, BSc

Heavy metal removal potential of natural and synthetic allophanes

MASTER'S THESIS

to achieve the university degree of

Master of Science

Master's degree programme: Earth Sciences

submitted to

GRAZ University of Technology

Supervisor:

Andre Baldermann, Dr.rer.nat.

Martin Dietzel, Univ.-Prof. Dipl.-Min. Dr.rer.nat.

Institute of Applied Geosciences (IAG)

Graz, September 2021

AFFIDAVIT

I declare that I have authored this thesis independently, that I have not used other than the declared sources/resources, and that I have explicitly indicated all material which has been quoted either literally or by content from the sources used. The text document uploaded to TUGRAZonline is identical to the present master‘s thesis.

_____ _____

Date Signature

Acknowledgments

First and foremost, I would like to thank my thesis supervisor, Dr. Andre Baldermann. The enthusiasm he showed in teaching clay science encouraged me to ask him to be my supervisor and I'm grateful that he gave me the opportunity and suggestion for this exciting topic. He offered me guidance and support throughout the time I was working in the lab facilities. Also afterwards, when I was writing on my thesis, he never hesitated to reserve time for me when I asked for advice. I benefited greatly from his meticulous editing and valuable suggestions that reminded me to stay focused.

I would like to acknowledge Prof. Martin Dietzel for inspiring my interest in mineralogy and hydrogeochemistry already in the early stage of my studies; it was always a pleasure to attend his lectures. I also want to thank Prof. Dietmar Klammer; even though I haven't been on campus for years, his nice greeting and welcome when we met made me feel as though I had only been away for a week.

My thanks go to Maria Hierz and Andrea Wolf who introduced and encouraged me to the laboratory work; with profound knowledge they gave me dedicated support in preparing and conducting my experiments and I'm grateful for their encouragement and help.

Last but not the least I would also like to thank my husband and my son for being patient.

Abstract

Synthetic allophanes (“s1” and “s2”, Al/Si molar ratio 1.0) and a natural allophane (“n”, Al/Si molar ratio 1.3, from Ecuador) were studied related to their performance in adsorption of aqueous barium (Ba), cobalt (Co), strontium (Sr) and zinc (Zn) as a function of contact time and pH (pH range 8.5 to 4.0). Mineralogy, nanostructure, particle form, chemical composition and specific surface area of the allophanes were characterized by Fourier transformation infrared spectroscopy, X-ray diffraction, transmission electron microscopy and specific surface area measurements. Kinetic experiments revealed that a steady-state between adsorption and desorption processes is reached within the first 10 min, the evolution of adsorption fitted to pseudo-first-order kinetics. Adsorption performance was best at pH 7.5 to 8.5; the performance showed pH dependency for all allophanes. Although, especially the “s1” and “s2” demonstrated acceptability for removing aqueous metals over a wide pH range. Natural “n” is also a good candidate for uptake of metal ions, for “n” a usage in environments with more restricted pH variation (pH 7.5 to 8.5) is recommended.

Kurzfassung

Untersucht wurde das Adsorptionsverhalten zweier synthetischer Allophane (“s1” und “s2”, Al/Si-Molverhältnis = 1.0) sowie eines natürlichen Allophan-Rohmaterials (“n”, Al/Si-Molverhältnis = 1.3, aus Ecuador) in Bezug auf die in wässriger Phase gelöst vorliegenden Spezies der Metalle Barium (Ba), Kobalt (Co), Strontium (Sr) und Zink (Zn) in Abhängigkeit von Kontaktzeit und pH Wert (im Bereich von pH 8.5 bis 4.0). Die Mineralogie, Nanostruktur, Partikelform, chemische Zusammensetzung und die Spezifische Oberfläche der Allophane wurde mithilfe von Fourier-Transformations-Infrarot-Spektroskopie, Röntgenpulverdiffraktometrie, Transmissionselektronenmikroskopie und Methoden zur Ermittlung spezifischer Oberfläche mittels Stickstoffadsorption bestimmt. Die kinetischen Experimente ergaben, das sich bereits innerhalb der ersten zehn Minuten ein dynamisches Gleichgewicht zwischen Adsorptions- und Desorptionsprozessen an den Allophanen einstellte. Die Kinetik der Adsorption konnte einer pseudo-erster Ordnung Kinetik zugeordnet werden. Alle Allophane zeigten ein pH-abhängiges Adsorptionverhalten mit höchsten Werten zwischen pH 7.5 und 8.5. Dabei zeigten vor allem die synthetischen Allophane „s1“ und „s2“ eine hohe Eignung um Metalle über einen weiten pH Bereich zu adsorbieren. Der natürliche Allophan „n“ ist ebenfalls gut für die Aufnahme von Metallspezies geeignet, auch wenn hier die Verwendung in einem Umfeld mit geringerer Variation des pH-Werts (pH 7.5 bis pH 8.5) empfohlen wird.

Table of Contents

[1]This chapter is published in *Geosciences*, **8**, 309: Baldermann et al. (2018).

[1]This chapter is published in *Geosciences*, **8**, 309: Baldermann et al. (2018).

1. Introduction

Worldwide, mining, agricultural, urban and industrial activities have left behind hazardous matters in the environment, such as plant nutrients (nitrogen, phosphorus, potassium), pathogenic microorganism (viruses, bacteria, protozoa and helminths), heavy metals (e.g. cadmium, chromium, copper, mercury, nickel, lead and zinc), organic pollutants (e.g. polychlorinated biphenyls, polyaromatic hydrocarbons, pesticides) and biodegradable organics (BOD, COD), and micro-pollutants (e.g. medicines, cosmetics, cleaning agents) (UN-water, 2015). Due to increasing anthropogenically-driven water pollution, the availability of drinking water and (ground)water of acceptable quality is on risk in many countries (United Nations, 2009). Untreated wastewater causes plenty of negative impacts on human health, the environment and productive activities as, for instance, the risk of disease due to contaminated drinking water and food, a decreasing biodiversity and degraded aquatic ecosystems, and a reduced industrial and agricultural productivity. Besides prevention or reduction of pollution levels at the source of contamination, the removal of contaminants from wastewater streams is of great importance to enable a safe use of the treated water (i.e. water reuse) under controlled conditions for beneficial purposes. Additional to the historical primary use for irrigation, advanced treatment technologies provide higher quality of the effluent water that also allows for other uses (United Nations, 2017).

Besides the natural release of contaminants, such as heavy metals, by weathering processes of rocks and minerals, these are among the most important water contaminants created by human activities (United Nations, 2009). That made demands on scientific and technical communities to investigate materials and to develop appropriate treatments that are able to remove toxic and/or cancerogenic heavy metals from water resources, sediments and soils (Yuan & Wada, 2012). An emerging area of research is the development of nano-materials, which can act as a substrate (authors note: by sorption processes) to enhance the removal of distinct heavy metals from water supplies (United Nations, 2009). The natural occurring nano-sized clay mineral allophane, a short-range-order aluminosilicate phase with the composition $Al_2O_3 \cdot (SiO_2)_{1.3\text{-}2} \cdot (2.5\text{-}3.0)H_2O$, is a good candidate material to be used for wastewater treatment and water conditioning since it has already been proven to have a high removal potential for diverse aqueous metallic and organic contaminants (Yuan & Wada, 2012). Various studies have been published with focus on describing allophanes outstanding characteristics, like large surface areas of up to ~900 m^2/g (Iyoda et al., 2012) with the ability to carry both positive and negative surface charges at the same time (e.g. Yuan & Wada, 2012). Studies that concentrate on the investigation of adsorption abilities often take less focus on identifying the required equilibrium time and the optimal contact time between adsorbents and experimental solutions (Tran et al., 2017). In many studies, the pH effect is invariably examined only in terms of the initial pH of solutions, and, although it is well known that metal ion adsorption is pH dependent, changes of pH during the course of experiments are not often demonstrated (Tien, 2008).

The main focus is the investigation of the adsorption of heavy metals on allophane at variable solution pH by a comparison of adsorption efficiency (% removal) of natural vs. synthetic allophanes.

In this study, the results of kinetic an pH-drift experiments are presented, where allophane was brought into thermodynamic equilibrium (e.g. chemical steady state) with a series of artificial wastewater solutions. The capability of allophanes related to the uptake of aqueous species of a defined selection of heavy metals (Ba, Co, Sr, Zn) was tested on two types of materials: two synthetic allophanes and an allophanic raw material, mined from a natural environment in Ecuador. Effort was taken to characterize the natural and synthetic allophanes by various analytical techniques, including infrared (FTIR) spectroscopy, X-ray diffraction, transmission electron microscopy (TEM) with energy dispersive X-ray spectroscopy (EDX), and Brunauer-Emmett-Teller (BET) method, in attempt to relate the main compositional, nano-structrual, mineralogical and physical features of allophane with measured adsorbent performances.

2. Allophane and Related Minerals

2.1 Literature Review

The mineral allophane was first described by Hausmann & Stromeyer (1816). The "soil-like" mineral originated from a deposit in Thuringia (Germany), and subsequent chemical analysis determined the main components of allophane to be water, "Alaunerde" and silica (Hausmann & Stromeyer, 1816). "Alaunerde" or "Tonerde" are German terms for aluminium oxide, which was known since long time, although the native aluminium wasn't proven at that time. A synonym for allophane is riemannite; named after Riemann, who first observed the mineral (Breithaupt, 1817). Different from the assumption to be a mineralogical rarity of the location (Breithaupt, 1817), descriptions of allophanes from other locations in Germany and Poland followed. It was proposed that allophane forms through secondary processes that may continue until recently (i.e. von Leonhard, 1826) and, hence, it is frequently assumed to be of allochthonous origin in soils and sediments. Evidence for a young formation within only a few hundred years saw Breithaupt (1829) in the discovery of allophane from Freiberg (Saxony, Germany); there it appeared as incrustation of unalterated wood (author's note: authigenic or in situ formation), and, first for the time, small and easy to squash crystals were found. However, more than 100 years later, allophane was defined as an amorphous material with no ordered crystal structure (i.e. Ross & Kerr, 1934). In the 1950s and 1960s, and due to arising problems lots of clayey soils (i.e. volcanic ash soils) caused in soil engineering practice, investigations were done with the intention to better define the properties, structure and chemical composition of clay minerals in general (Birrell & Gradwell, 1956; K. Wada & Ataka, 1958). Meanwhile, allophane was found nearly all over the world, especially in developing volcanic soils. Earlier studies didn't distinguish between allophane- and imogolite-type clay minerals. However, with increasing methodological and technical possibilities, like for instance the progress in electron microscopy and spectroscopic techniques, definitions of clay minerals had to be changed over time. Investigations on the properties of allophane made progress and revealed its outstanding characteristics, especially in terms of its hollow nanoball structure and complex ways of ion uptake from solution (Farmer et al., 1979; Henmi & Wada, 1976; Parfitt et al., 1980; Parfitt & Henmi, 1980).

Today, natural (and synthetic) allophane and imogolite nano-particles are very attractive from a technological and economic viewpoint due to high availability, low costs, good performance and safety use in environmental and health studies, and technical applications. They are used in e.g. versatile functions as adsorbents, filters, catalysts and carbon stabilisers, and they are increasingly involved e.g. in providing essential ecological services, ranging from regulating water storage and nutrient (re)cycling through adsorption and transportation of aqueous metal ions and organic contaminants (Yuan & Wada, 2012).

2.2 Morphology, Structure and Chemical Composition

2.2.1 Basics and Important Terms

Structure of Layer Silicates (Phyllosilicates)

Fundamental features that are leading to the different behaviours of layer silicates in different natural or technical processes have been published by Brigatti et al. (2011), that study is the reference for the following text:

The idealized structure of layer silicates (a layer by definition) is the build up by repeated stacking of **tetrahedral (T) and octahedral (O) sheets.** The way of repetition of T and O sheets along the crystallographic c direction gives a classification of layer silicates. TO stacks form 1:1 layer silicates (the unit cell consists of six octahedral and four tetrahedral sites), whereas TOT stacks lead to 2:1 layer silicates (the unit cell is characterized by six octahedral and eight tetrahedral sites). Additional, mixed-layer (or interstratified) phyllosilicates with layers of different structures and/or compositions exist that are alternated with some sort of ordering or random distribution. Indeed, many distortions and deviations (e.g. by chemical substitutions) from ideal structures may occur. **The T sheet** (Figure 1a) consists of individual TO_4 tetrahedra (with tetrahedral cation T in centre, usually Si^{4+}, Al^{3+}, Fe^{3+}) that are interconnected by sharing three basal corners (basal oxygen, Ox_b) of each tetrahedron. The result is an infinite 2-dimensional 'hexagonal' ring pattern when viewed along the crystallographic a and b axes. There, electrically neutrality is established when all tetrahedra contain Si^{4+} in central position. **The O sheet** (Figure 1b) consists of octahedra that are interconnected by sharing anions at the edges (octahedral anion Ox_o: OH, F, Cl), creating a hexagonal or pseudo-hexagonal symmetry. The centre of an octahedron is usually occupied by a cation (octahedral cation O, usually Al^{3+}, Fe^{3+}, Mg^{2+}, Fe^{2+}). On the basis of half unit cell content, electrical neutrality within the octahedral sheet can be established by two different configurations that are defined by the charge and size of the central cation: (1) two of three sites (2/3, dioctahedral) are filled with trivalent cations (Al^{3+}, Fe^{3+}) and the third site is vacant; (2) all sites (3/3, trioctahedral) are filled with bivalent (Mg^{2+}, Fe^{2+}) cations. **The connection of T and O sheets** (Figure 1c) is realized by sharing of the apex of the tetrahedra: this fourth oxygen atom (apical oxygen Ox_a) forms a corner to the octahedrons of the O sheet. For the built-up of a continuous octahedral sheet, all free apical oxygen atoms of the tetrahedra need to be oriented to the same direction of the T sheet. Otherwise, only octahedral 'ribbons' are connected to the T sheet (i.e. sepiolite, palygorskite). **The layer charge** of the joined TO or TOT sheet structure can either be neutral (ideally) or negative; it is produced by the sum of charges of the individual sheets. Within tetrahedral sheets a negative charge arises by substitution of Al^{3+} for Si^{4+} in central position. Regarding octahedral sheets, a negative charge arises by substitution of lower-charge cations and when vacancies are present in trioctahedral (3/3) spe-

cies. The location of the (negative) layer charge is important, since the charge of tetrahedral basal oxygen atoms, which build both outer surfaces of a TOT layer (Ox_b, Figure 1c), is most affected by the imbalance when it is located in the T sheet. **Interlayer sites** that separate two adjacent layers can be empty or occupied by cations, hydrated cations, organic material, hydroxide complexes, and/or hydroxide octahedral sheets. For instance, the dioctahedral **1:1 clay minerals of the kaolin subgroup** with (ideally) neutral layer charges show relatively weak bonds between adjacent layers. The interlayer space of kaolinite is empty; additional to bonding by van der Waals forces, the TO layers are kept together by hydrogen bridges between outer surface hydroxyl group (Ox_o) of the O sheet and basal oxygen atoms (Ox_b) of the T sheet. Indeed, structural dislocations (e.g stacking faults) and isomorphic substitutions in T and O sheets of kaolin minerals are common. Halloysite-10 Å (1:1, dioctahedral) is a hydrated member in the kaolin subgroup; the space between the adjacent TO layers is filled with intercalated water molecules that can easily be removed. Especially for **2:1 layer silicates**, the layer charge is a fundamental property that influences physical and mechanical hardness. The softest minerals are talc and pyrophyllite; the ideal layer structure of both is electrically neutral, and adjacent TOT layers are only connected by weak van der Waals forces. For **mica group minerals** (e.g. muscovite, phlogopite), a negative charge arises by substitution (Al^{3+} for Si^{4+} in a ratio near to 1:3) within the T sheet. To balance the arising negative charge, fixed cations (e.g. K^+) usually fully occupy the interlayer site; they maintain compact layers (layer spacing ~10 Å) and strong bonding of adjacent layers. By contrast, for most **2:1 clay minerals** the interlayer sites are not fully occupied, and sometimes, they are hydrated. The clay minerals of the **smectite group** (e.g. montmorillonite, saponite) show permanent negative layer charge (by substitutions in T or O sheet), which is compensated by commonly hydrated and exchangeable cations in the interlayer. Higher (negative) layer charge results in a higher number of intercalated cations, which is accompanied by higher total hydration and, hence, increasing layer spacing (crystalline swelling). Clay minerals of the **vermiculite group** also present hydrated exchangeable cations in the interlayer position to balance the negative layer charge (usually Al-for-Si substitutions in T sheet). This is greater than observed in smectite, and, hence, vermiculite minerals hydrate more strongly. Finally, **chlorite group minerals** basically exhibit a 2:1 layer; however, to balance the total negative charge of the 2:1 layer, a brucite-like octahedral interlayer sheet with positive charge separates the adjacent 2:1 layers (also known as 2:1:1 structure) (Brigatti et al., 2011).

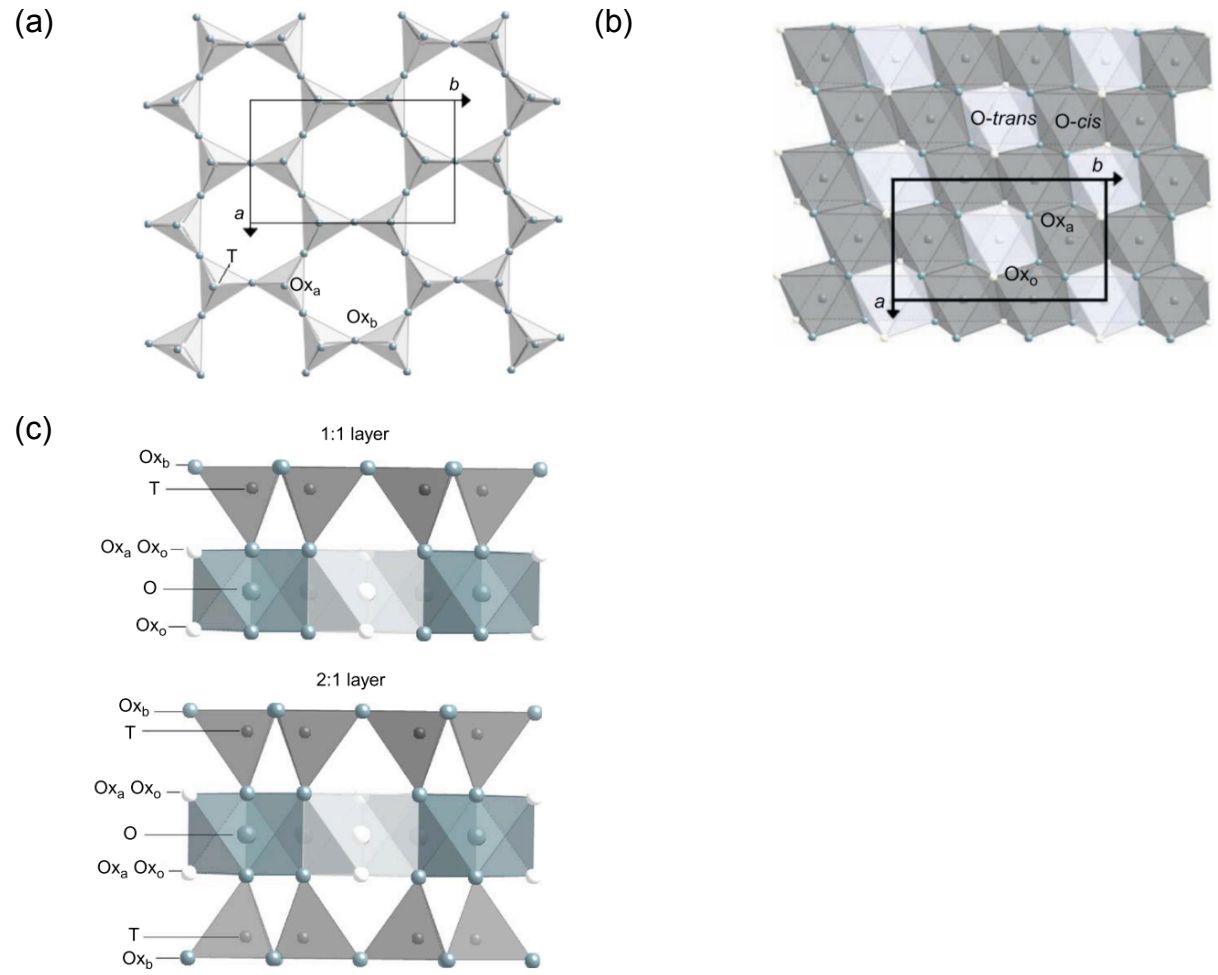

Figure 1. Overview of the different building units of layer silicates, a and b refer to unit-cell parameters. ***(a)*** *Tetrahedral (T) sheet. T: tetrahedral cations (Si^{4+}, Al^{3+}, Fe^{3+}); Ox_a: apical oxygen atoms; Ox_b: basal oxygen atoms.* ***(b)*** *Octahedral (M) sheet with O-trans (trans- oriented octahedral) and O-cis (cis-oriented octrahedra) topology that is depending on Ox_o octahedral anions (OH^-, F^-, Cl^-) positions. Ox_a: apical oxygen atoms.* ***(c)*** *Models of 1:1 and 2:1 layer structures (Brigatti & Gala, 2013).*

Short-range order

In general, all solids exhibit short-range order, since this is substantiated by the concept of atomic bonding. If a mineral is called "short-range ordered", the highest order occurring in this matter is at the atomic scale. The term **short-range order (SRO)** describes the structural organization associated with the first coordination shell around a given origin atom (Elliott, 2001). The SRO of silicates is typically modelled as a $[SiO_4]^{4-}$ tetrahedral anion with a silicon atom in the centre, which is surrounded by 4 oxygen atoms (quaternary species). In case of aluminosilicates, aluminium (Al^{3+}) replaces some of the silicon (Si^{4+}) in central tetrahedral position. As a consequence, the charge of these tetrahedrons gets more negative $[AlO_4]^{5-}$) and a difference of a single negative charge arises. This negative charge and the different ways to compromise for it, account for the high variety of different clay mineral structures, and for the special properties of the different groups of silicates.

Nonbridging oxygen-containing quaternary silicate species

The term **NBO (nonbridging oxygens**) is related to the oxygen atoms that build the corners of the SRO of quaternary silicates. An oxygen atom is called NBO, if it is not linked to other tetrahedrons, like it is implied for the formation of polymeric silicate molecules. NBO-containing silicate species (Figure 2) are referred to as quaternary species Q_n, where n (= 0 - 4) is the number of bridging (doubly coordinated) oxygen atoms in the tetrahedral coordination polyhedral centred on silicon atoms of silicates (Elliott, 2001). With higher numbers for Q_n, the polymerization and complexity of the silicate network increases.

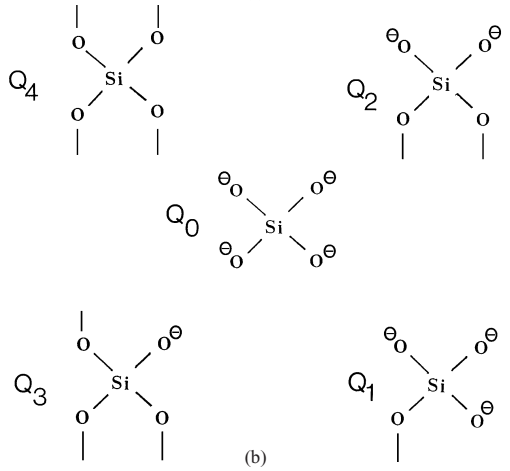

Figure 2. Overview about different polymerization degrees of silicates based on the concept of bridging and nonbridging oxygen atoms via corner-shared Q_n NBO (nonbridging oxygens) species (Elliott, 2001).

2.2.2 Allophane and Imogolite

Allophane and imogolite are hydrated and strongly curved natural nanoparticles. They are commonly assigned to poorly crystalline or short-range order (SRO) aluminosilicates. However, their structure varies significantly from that of other clays, such as illite and smectite group minerals (K. Wada, 1978). Moreover, attributing allophane and imogolite to clay-sized and short-range ordered minerals is rather a simplification. Indeed, a wide range of crystallinity occurs, from amorphous to crystals in size of several cm. For instance, allophane and imogolite with aggregate crystal sizes up to 10 cm in diameter can form by replacing tree roots in paleosols (Grathoff et al., 2003). Regarding their formation, occurrence and properties, allophane and imogolite are frequently directly related to each other. The distinction between the two minerals can be challenging since, related to their occurrence in weathering regimes, numerous additional phases (often amorphous) in natural soils are common. Especially in case of allophane the variety in structure and chemical composition is high, and, by this, its properties and structure are still under debate.

Allophane and imogolite are both classified as phyllosilicates (Dana 8th ed.: sheets of 6-membered rings; Nickel-Strunz 10th (pending) ed.) with kaolinite-type layers composed of tetrahedral and octahedral sheets, although their structure differs strongly. Electron micrograph studies brought evidence that imogolite is composed of fine aluminosilicate nanotubes with external and internal diameters of 20 Å and 10 Å, respectively, whereas allophane particles are spherical and hollow (appear ring-shaped) with an outside diameter of 35–50 Å and a wall thickness of 10 Å or less (Henmi & Wada, 1976; S.-I. Wada & Wada, 1977). The observed fine tubes of imogolite confirm that imogolite, additional to its short-range order, possesses long-range order at least to some degree, but primarily in one crystallographic direction. The ideal chemical formula of natural imogolite is $(OH)_3Al_2O_3SiOH$, implying an Al/Si molar ratio of 2, hence contrasting the formula of allophane, which varies in the range $Al_2O_3 \cdot (SiO_2)_{1.3\text{-}2} \cdot (2.5\text{-}3.0)H_2O$.

Table 1 shows the attempt of Levard et al. (2012) to give an outline of findings regarding SRO aluminosilicate variants from several authors. Complemented with their own results, they have supposed a representative nomenclature for short-range ordered aluminosilicates that includes imogolite and allophane and their varieties based on chemical compositions and atomic structures obtained from different analytical techniques. The use of a combination of different techniques for SRO-mineral classification is recommended, because of the fragility of allophane and imogolite group minerals under a conventional electron beam (Levard & Basile-Doelsch, 2016). The Al/Si ratio is an important criterion for the definition of allophane and imogolite (Table 1), which can be identified e.g. by NMR (nuclear magnetic resonance; ^{29}Si, ^{27}Al). Imogolite (and also its precursors) has a relative constant Al/Si ratio of approximately 2. For allophane, a higher variety in chemical composition from Al/Si = 0.9 to 4 is possible; its structure is more miscellaneous than that of imogolite. Spectroscopic methods (like FTIR) are also useful for their identification since differences in the structure between imogolite, Si-rich allophane and Al-rich allophane can be detected. Indeed, Al-rich allophanes and proto-imogolites are not dissociable (Levard et al., 2012): **IR bands between 930 and 995 cm^{-1} belong to imogolite** and its precursors. Accordingly, an IR band **at 970 cm^{-1} corresponds to Al-rich allophane** (also known as proto-imogolite). Contrary, IR bands **between 1000 to 1100 cm^{-1} belong to Si-rich allophane and to silica-spring allophane.** Silica-spring allophane, related to a formation in rivers and springs, has a more polymerized structure compared to allophanes of volcanic origin. In contrast to imogolite and Si- and Al-rich allophane, silica-spring allophane does not contribute to imogolite-type materials.

Table 1. Nomenclature, occurrence and structure of short-range ordered aluminosilicates reported in the literature (after Levard et al., 2012).

	Imogolite		Allophanes			
	Imogolite	*Precursors*	*Silica-spring*	*Si-rich allo*	*Al-rich allo*	*Precursors*
Other Name		proto-imogolite allophanes	feldspathoit allophanes		proto-imogolite allophanes	
Natural occurrence	pumice and andosols	?	spring river bed	pumice and andosols	pumice and andosols	?
Shape	nanotubes	tile shape particles	spherules fragment	spheres ovoids ?	spheres ovoids ?	?
	Characteristics features for commonly used techniques					
	Imogolite		Allophanes			Identification
	Imogolite	*precursors*	*Silica-spring*	*Si-rich allo*	*Al-rich allo*	
Chemical comp. (Al/Si)			0.9–1.8	≈1		Si-rich
	≈2	≈2			≈2 (up to 4)	Al-rich
^{29}Si NMR (ppm)	−78	−78	−78	−78	−78	Q0
			−80 to −110	−80 to −110		Q1 to Q4
^{27}Al NMR (ppm)	5–6	2–6	2–6	2–6	2–6	Al ^{VI}
			55	55		Al ^{IV}
	930 and 995	970		1000–1100	970	Si—O strteching
FTIR (cm^{-1})	425, 500, 570 325 and 690	425, 500, 570	425, 500, 570	425, 500, 570	425, 500, 570	ILS tubular
XRD (Å)	2.2 and 3.4 8.4 and 20	2.2 and 3.4	2.2 and 3.4	2.2 and 3.4	2.2 and 3.4	ILS (001) and (100)
TEM	nanotubes	amorphous	?	spheres, rings ?	spheres, rings ?	

2.2.3 Imogolite-Type: Si-rich and Al-rich Allophanes

The term imogolite-type material includes all short-range ordered aluminosilicates having (in part or totally) an **Imogolite-Local-Structure (ILS**), even with more or less amorphous character (Levard et al., 2012). This definition holds true for imogolite and Al-rich allophanes (Figure 3A). In contrast to the condensed (or polymerized) tetrahedrons (silicon in Q_3 configuration) in most layer silicates, the ILS contains abundant isolated silicon sites in Q_0 configuration. ^{29}Si-NMR spectroscopy can be used to detect ILS in soils and solutions since shifts in Q_n configuration are sensitive for and representative of the degree of condensation of tetrahedral networks (Barron et al., 1982). The local structure of Si-rich allophane (Figure 3B) is quite similar to the ILS. Although, with increasing Si content (decreasing Al/Si ratio), increasingly more tetrahedrons are added at the inner surface to the ILS by shearing oxygen corners; hence, the amount of polymerized Q_1 to Q_4 silicon species increases (Levard et al., 2012).

Figure 3B and 3D reveal the morphology of imogolite and Si-rich/Al-rich allophanes, respectively. Both exhibit an open structure, which accounts for the accessibility of their inner caves, for instance, for appreciable amounts of water (Kaufhold et al., 2010). The wall perforations of the allophane allows for rapid exchange of water between outer and inner space (Parfitt & Henmi, 1980). They are, hence, very important for the sorption performance of allophane (Chapter 6.2).

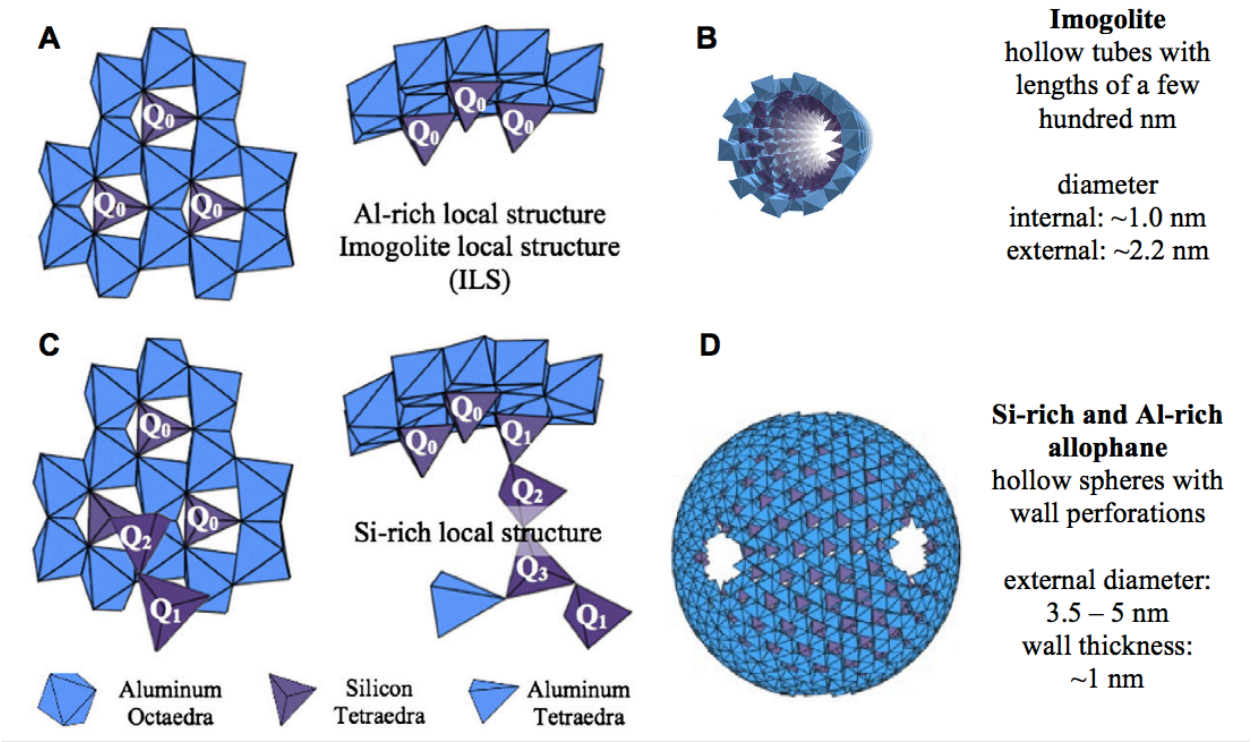

*Figure 3. Local structures of Al-rich **(A)** and Si-rich **(C)** short-range ordered aluminosilicates. The Al-rich local structure is equal to the Imogolite Local Structure (ILS). The Si-rich local structure differs in additional appearance of polymerized tetrahedrons. They are denoted Q_n, where n (ranging from 0 to 4) stands for the number of directly linked silicon tetrahedrons. **(C)** Primary imogolite particle. **(D)** Primary Si-rich and Al-rich allophane particles (adapted after Levard et al., 2012; Levard & Basile-Doelsch, 2016).*

2.2.4 Non-Imogolite-Type: Silica-Spring Allophane

Silica-spring allophane (or stream deposit allophanes) precipitates in rivers and streams but is barely observed (Levard & Basile-Doelsch, 2016). Although it is called allophane, its structure strongly differs from the allophanes described before. The difference can be seen in Figure 4 (Rampe et al., 2011): In contrast to Al-rich allophanes, where a continuous dioctahedral gibbsite-like layer builds the outer surface and (more or less) isolated tetrahedra are connected to in the inner surface, the layers of silica-spring allophanes are arranged in reverse order. Here, a polymerized tetrahedral sheet, where Al^{3+} partially substitutes for Si^{4+}, builds the outer surface, which is linked to discontinuous alumina octahedral sheets that build the inner surface. Silica-spring allophanes have Al/Si ratios from 0.9 to 1.8 with the morphology of more or less complete spherules with diameters of ~2-3 nm (Childs et al., 1990). Because of the polymerized tetrahedral sheet, Si is not present in Q_0 configuration. Hence, the silica-spring allophane does not belong to the imogolite-type material family (Levard & Basile-Doelsch, 2016).

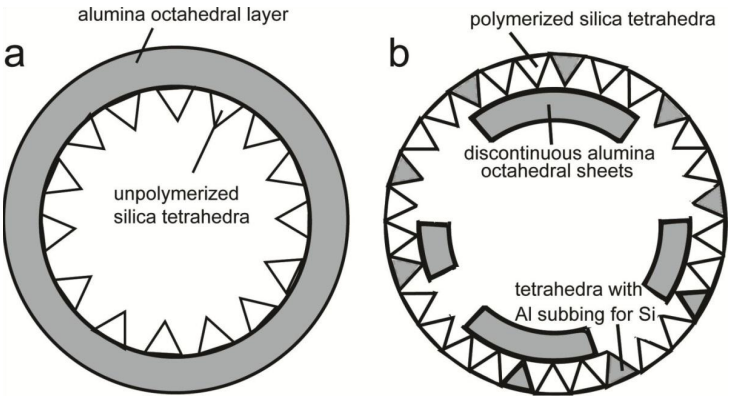

Figure 4: Comparison of allophane structures. a) Al-rich allophane (here called imogolite-like allophane); b) Silica-spring allophane (here called stream deposit allophane) (Rampe et al., 2011).

2.3 Formation Conditions and Stability

The natural occurrence of allophane and imogolite group minerals is typically related to weathering regimes and developing soil profiles. These metastable products are formed in favour of more stable crystalline minerals (such as kaolinite), because the lower surface tension of SRO materials enables them to nucleate more rapidly in aqueous solutions (poorly crystalline → highly reactive). Although they are metastable, they may exist for a long period of time, like over tens of thousands of years, before they may transform to more crystalline minerals (Harsh, 2005). Hence, allophane and imogolite group minerals may be partly seen as precursors of kaolin-type clay minerals. It is generally accepted that allophane and imogolite precipitate in relatively acidic solutions that percolate downwards from upper soil horizons (like the eluvial horizon). In case of allophane, formation might be associated with the in-situ transformation of parent material (like pumice) or the result of (co-)precipitation from an oversaturated percolating solution (Levard et al., 2012).

According to Harsh (2005), available and sufficient amounts of dissolved Al and Si or reactive siliceous materials are the main drivers for allophane and imogolite formation. Their occurrence is not restricted to a specific environment or parent material since a rapid ability of Al and Si can be established in different ways, for instance, by the alteration of labile parent materials, such as volcanic ash in tephra and pyroclastics. Here, the amorphous character and fine particle size of the vitreous parent material account for a high solubility and enhance the weatherability, allowing for a fast conversion into volcanic soils, preferentially in a moderate humid climate. In spite of their abundance in the soils mentioned before, to which allophane and imogolite are commonly associated with, several findings confirmed the existence of allophane and imogolite in soils that are not related to volcanism. Intense weathering of any siliceous parent materials that can provide a rapid ability of dissolved Al and Si can lead to the formation of allophane and imogolite (Harsh, 2005).

2.4 Properties and Relevance for Natural Environments

Allophane is known for its large specific surface areas (>> 100 m^2/g) and high chemical reactivity (K. Wada, 1978). Responsible for the high surface area is the nano-sized and porous structure of allophane (Michot, 2018). Given by the huge surface that is assembled with high amounts of functional groups (i.e. aluminol and silanol), chemical and physical reactions, like adsorption, are promoted on outer and inner surfaces. Allophane is able to adsorb appreciable amounts of water and ionic substances, similar to minerals of the smectite group. However, allophanes can incorporate water molecules only in the inner part of the hollow sphere without an increase of the unit cell, typically in crystallographic c direction (e.g. Kaufhold et al., 2010). Allophane (and imogolite) can concurrently have both positive and negative (permanent or impermanent) charges. They are able to adsorb cations, anions and organic molecules, which make allophane- and imogolite-type materials popular for industrial application (Iyoda et al., 2012; Yuan & Wada, 2012). For more details about adsorption properties, see Chapter 6.2.

Allophane plays an important role for the stabilisation of organic matter (OM) in soils. OM that is sorbed on clay surfaces or inaccessible within pores is protected from microbial decomposition. Thus, allophane is of value for the retention of nutrient cations, anions and heavy metals in soils and, thus, important for agriculture and environmental protection. Negatively charged OM is frequently sorbed onto allophane surfaces by ligand complexation mechanisms, whereas positively charged organic ions mainly occupy parts of pore space by physical adsorption (e.g. Parfitt, 1990). Allophanic soils are also of interest in terms of controlling the greenhouse effect by carbon sequestration since it is proven that the carbon content in allophanic soils is positively correlated to the allophane content (Chevallier et al., 2008).

3. Materials

Adsorbent Materials: The tested materials are synthetic allophanes, synthesized following a procedure described in Chapter 4.1; and a natural allophane, won from a natural soil environment in Ecuador. The natural allophane raw material, kindly provided by BGR (Bundesanstalt für Geowissenschaften und Rohstoffe, Stilleweg 2, D-30655 Hannover, Germany), originates from a massive allophane-rich layer in Santo Domingo de los Colorados in Ecuador. This deposit was found in the late 1980s; it covers an area of >4000 m^2 and has a general thickness of >5 m. Because of its high quality (important criteria: high allophane content, thickness of the allophane layer, small amount of organic carbon) and low price, the material is currently being tested for various industrial applications and for the production of novel nano-materials (Kaufhold et al., 2009). "Sample 4-7" comes from a profile termed "PM-4" and it was sampled in 6 m depth below the surface. The sample was kept moist and arrived at the IAG/TU Graz as a dilute suspension. The suspension was washed with ultrapure water and prepared for the adsorption experiments, using the same procedures as for the synthetic allophanes, which are described further below.

Chemicals and Laboratory Conditions: Unless stated otherwise, all methods were carried out at room temperature in lab facilities at the IAG/TU Graz. All chemicals and re- agents were of analytical grade and were used as received. Ultrapure water (Milli-Q Plus UV, Millipore, Burlington, MA, USA) with a resistivity of 18.2 MΩ at 25 °C was used for preparation of experimental solutions. For aqueous solutions, the density was assumed to be equal to water. Hence, the units mg/kg and ppm were used equivalent to mg/l. Since some of the metals in experimental use carried a potential health risk, caution was taken during handling, and all contaminated matters and liquids were collected and disposed of as hazardous waste.

[1]This chapter is published in *Geosciences*, **8**, 309: Baldermann et al. (2018).

4. Experimental[1]

4.1 Synthesis of Allophanes[1]

The aim of the synthesis experiments was to precipitate pure allophanes with an Al/Si molar ratio of 1. The experimental set up was based on the one proposed by Wada, Eto, & Wada (1979). However, slight modifications were done (e.g.: use of polymeric metasilicate instead of monomeric orthosilicate) and different Al salt sources were used. It was opted for a relatively high amount of stock solution (1000 mg) to have sufficient amounts of precipitate needed for the further adsorption experiments. **Reagents** (Table 2)**:** Adequate amounts of sodium metasilicate pentahydrate (Na_2SiO_3 * $5H_2O$, purchased from Roth) were mixed with 918 ml of ultrapure water to obtain a 109 mmol/l Si stock solution, which was stirred (magnetic stirrer) in a crystallisation chamber (Nalgene™ Straight-Sided Wide-Mouth Polycarbonate Jars with Closure, 1000 ml). Once the salt was dissolved, a pH of 12.8 was observed in the Si stock solution. Adequate amounts of an aluminium source and 82 ml of ultrapure water were added to the Si solution to obtain a solution containing 100 mmol/l Al and 100 mmol/l Si. Immediately, a reaction was observable by the precipitation of a white matter and a drop in pH to a value of around 3.92. **Establishment of pH 6:** To yield a high precipitation quota of Al and Si, the pH was re-adjusted to pH 6 by titration of sodium hydroxide solutions c(NaOH) = 2 mol/l (2 N) and c(NaOH) = 1 mol/l (1N). **Ageing:** Once the desired pH was reached, the reactor was closed and the suspension was stored at 90 °C for 48 h in a compartment dryer. **Further Preparation:** After ageing, the solids appeared as white gel and were concentrated at the bottom, whereas the almost clear liquid phase was on top of the reactor. A liquid sample was taken (for ICP-OES, Chapter 5.2.2) to verify the Al/Si molar ratio in solution and to back calculate the composition of allophane; it was filtered immediately (0.45 µm cellulose acetate). Afterwards, the supernatant was separated by decantation. In order to remove electrolytes (such as NaCl) from allophane surfaces, approximately 50 ml of the suspension (gel + remaining liquid) were mixed with 200 ml ultrapure water. The suspension was filtrated using a suction filtration unit, equipped with a 0.45 µm cellulose acetate filter. The material remaining on the filter was washed with 100 mg ultrapure water two times to obtain a target electrolyte concentration below 500 µS/cm (actually, the final EC was in the order of ~26 µS/cm). Afterwards, the gel-like precipitate was removed from the filter and collected in an evaporating dish. This described procedure was repeated until the whole gel-like phase was separated. Finally, the washed precipitate was dried at 40 °C, and pounded in a mortar to produce a soft powder. The collected liquid sample was acidified to a 2% HNO_3 matrix for the further ICP-OES analysis. Dilution was carried out in two steps (1st: dilution factor 50, 2nd: dilution factor 10) to get a final dilution factor of 500. The dilution factor was chosen in order to reach a sufficient concentration / detection range for the elements of interest. A total of

[1]This chapter is published in *Geosciences*, **8**, 309: Baldermann et al. (2018).

four different synthesis procedures (Table 2) were performed in analogy to the procedures described before. In chronological order, the precipitation products were labelled as "vs_allo_1", "vs_allo_2", "s_allo_3" and "s_allo_4". The yield of ~15 g powder per synthesis was retained for solid-phase characterization and for use in subsequent adsorption experiments.

Table 2 Overview of reagents used for allophane syntheses, amount of precipitates, and blends for further experimental use. Blend s1 consists of 35 % precipitate derived from "vs_allo_1" and 65 % derived from "vs_allo_2". Blend s2 consists of 52 % precipitate derived from "s_allo_3" and 48 % derived from "s_allo_4".

reagents for synthesis				precipitates		blends from precipitates	
reagent Si	Si [mmol/l]	reagent Al	Al [mmol/l]	name	amount [g]	name	percentage [%]
$Na_2SiO_3 * 5H_2O$	85 ±5	$AlCl_3$	100	vs_allo_1	12.4	s1	35
$Na_2SiO_3 * 5H_2O$	100	$Al(NO_3)_3 * 9H_2O$	100	vs_allo_2	14.0		65
$Na_2SiO_3 * 5H_2O$	100	$AlCl_3 * 6H_2O$	100	s_allo_3	17.0	s2	52
$Na_2SiO_3 * 5H_2O$	100	$AlCl_3 * 6H_2O$	100	s_allo_4	14.9		48

ICP-OES Analysis of Residual Liquids: As stated in the synthesis protocol, the concentrations of Al and Si in residual liquids were analysed by ICP-OES. Table 3 lists the obtained data and, based on this, precipitation quota of allophanes. By the assumption, that all the removed Al and Si are finally incorporated in the resulting precipitates, the Al/Si molar ratios of the allophanes were calculated. The very high precipitation quotas indicate that almost all Al and Si in the synthesis stock solution were incorporated to build the allophanes. Hence, all four syntheses were successful as regards the efficiency of allophane production. The initial Al/Si molar ratio of 1 in the synthesis stock solutions is again confirmed in the precipitated allophanes; it supports that the Al/Si ratio largely governs the type of allophane that results (Harsh, 2005). The calculated Al/Si molar ratios of 1 for both "s1" and "s2" are in line with the results received from TEM-EDX analysis.

Table 3. ICP-OES data from residual liquids in use as basis for the calculation of Al/Si molar ratios in allophane precipitates and final blends.

	residual liquid				precipitate			blend/allophane	
	Al	Si	Al	Si	Al precip. quota	Si precip. quota	Al/Si molar		Al/Si molar (H. M.)
	[mg/l]	[mg/l]	[mmol/l]	[mmol/l]	[%]	[%]	[-]		[-]
vs_allo_1	5.0	6.0	0.18	0.21	98.76	98.68	1.001	s1	1.00
vs_allo_2	2.25	36	0.0832	1.3	98.6848	98.7	1.00		
s_allo_3	0.36	30	0.013	1.1	100.001	100.0	1.000	s2	1.000
s_allo_4	1.13	25	0.0418	0.90	100.0023	100.00	1.0000		

[1]This chapter is published in *Geosciences*, **8**, 309: Baldermann et al. (2018).

4.2 Adsorption[1]

4.2.1 Kinetic Study[1]

Studies of adsorption kinetics play an important role in identifying the required equilibration time and, hence, the optimal contact time for an adsorption process (Tran et al., 2017). The kinetic study was carried out as a basis for planning and interpretation of the subsequently conducted pH-drift experiments. In a first set of experiments, kinetic experiments at 25°C were conducted to identify the time required until thermodynamic equilibrium (e.g. chemical steady-state between adsorption and desorption reactions at the surface) between allophane adsorbent and the aqueous metal has been established, and to study the effect of contact time on the adsorption behaviour. Four respective metals (Ba^{2+}; Co^{2+}; Sr^{2+}; Zn^{2+}) and three allophanes (synthetic allophanes: "s1" and "s2"; natural allophane: "n"; Chapter 3) were tested at constant pH (8.5 and 5.5, respectively, each ± 0.1 pH units). The metal reagents are barium chloride dihydrate ($BaCl_2*2H_2O$, from Roth), cobalt(II) chloride hexahydrate ($CoCl_2*6H_2O$, from Roth), strontium chloride hexahydrate ($SrCl_2*6H_2O$, from Merck), and zinc chloride ($ZnCl_2$, from Merck). **Experimental Solution:** Adequate amounts of the respective metal salt to obtain 1 L metal stock solution with 10 mg/l metal and further 10 mmol/l sodium chloride (NaCl, from Roth) as background electrolyte were mixed with ultrapure water. The mixture was stirred (magnetic stirrer) in jars (1.5 L high-density polyethylene). **Addition of adsorbent:** 2 g of the respective allophane was added in solid form. **Establishment of pH:** Immediately after addition, the solution was adjusted to the respective pH value by titration of sodium hydroxide solution c(NaOH) = 0.1 mol/l (0.1 N) and hydrochloric acid c(HCl) = 0.05 mol/l (0.05 N), respectively. **Sampling:** At specified times (10 s, 30 s, 1 min, 3 min, 5 min, 10 min, 1h, and 1 day) liquid samples (for ICP-OES, Chapter 5.2.2) were taken (~ 1mL) using a syringe. Each sample was filtered immediately (45 µm cellulose acetate). The samples were acidified using HNO_3 of suprapure grade (Roth, ROTIPURAN®, Karlsruhe, Germany). **Data Proceeding:** Adsorption capacity (q_e, amount of adsorbate uptake per mass of allophane at equilibrium [mg/g]) was calculated according to Equation (1) (e.g. Tran et al., 2017) and adsorption efficiency (%removal, percentage of removed metal ions at adsorption equilibrium) was calculated according to Equation (2), where were C_0 is the initial concentration of the adsorbate [mg/l], C_e the equilibrium concentration of the adsorbate [mg/l], m the dry mass of adsorbent [g] and V the volume of adsorbate solution [L].

$$q_e = \frac{(C_0 - C_e)}{m} \times V \qquad (1)$$

$$\%removal = \frac{(C_0 - C_e)}{C_0} \times 100 \qquad (2)$$

[1]This chapter is published in *Geosciences*, **8**, 309: Baldermann et al. (2018).

4.2.2 pH-drift Experiments[1]

In a second set of experiments, a total of twelve pH-drift (equilibrium) experiments were performed to study the effect of pH on the uptake of aqueous metal ions by allophanes; four respective metals (Ba^{2+}; Co^{2+}; Sr^{2+}; Zn^{2+}) and three allophanes (synthetic allophanes: "s1" and "s2"; natural allophane: "n"; Chapter 3) were tested. The pH range from 8.5 to 4.0 was considered, chosen to cover conditions found in natural waters. The metal reagents are barium chloride dihydrate ($BaCl_2*2H_2O$, from Roth), cobalt(II) chloride hexahydrate ($CoCl_2*6H_2O$, from Roth), strontium chloride hexahydrate ($SrCl_2*6H_2O$, from Merck), and zinc chloride ($ZnCl_2$, from Merck). **Experimental Solution:** From each of the four metals, three identical 1 L metal stock solutions were prepared (12 in total). That was done on the previous day (Co) and on the day of experiment (Ba, Sr, Zn), respectively. Adequate amounts of the respective metal salt to obtain 10 mg/l of the metal and further 10 mmol/l sodium chloride (NaCl, from Roth) as background electrolyte were mixed with ultrapure water. The solutions were stirred (magnetic stirrer, 300 rpm) in jars (Nalgene™ Straight-Sided Wide-Mouth Polycarbonate Jars with Closure, 1000 ml); pH, T and EC were monitored. **Sampling of Metal Solutions:** On day of experiment, liquid samples (for ICP-OES, Chapter 5.2.2) were taken for concentration analyses. **Addition of Adsorbent:** 2 g of allophane powder ("s1", "s2", or "n") were added in solid form to the respective metal solutions. The suspension got time to establish adsorption equilibrium, which took 1.5 h, and as a control for equilibrium conditions, the pH was observed. **Establishment of pH 8.5:** Once the pH was at a constant value (pH ~5-6 for adsorbent "n"; pH ~6-8 for adsorbents "s1" and "s2"), a starting pH of 8.5±0.07 was set by titration of a NaOH solution (0.1 N). Again, the suspension got time to equilibrate and a liquid sample was taken for chemical analysis. **pH-drift:** The pH was lowered by the dropwise addition of HCl solutions (0.1 and 1 N). At each pH step (intervals of 0.24 to 0.65 pH units) the experiments had sufficient time to equilibrate, following sampling of the liquid phase (as stated above) and repeating this procedure until pH 4±0.08 was reached. In total, of 12 (or 13) samples were taken per experiment. All liquid samples (1ml each) were filtered (0.45 µm cellulose acetate) immediately after sampling. The samples were acidified to a 2% HNO_3 matrix; the dilution factor was set to 20 for all liquid samples. **Data Proceeding:** Adsorption capacity (q_e) was calculated according to Equation (1) and adsorption efficiency (%removal) was calculated according to Equation (2), where were C_0 is the initial concentration of the adsorbate [mg/l], C_e the equilibrium concentration of the adsorbate [mg/l], m the dry mass of adsorbent [g] and V the volume of adsorbate solution [L].

[1]This chapter is published in *Geosciences*, **8**, 309: Baldermann et al. (2018).

5. Analytical Methods

5.1 Solid Phase Characterization

Solid phase characterization of the adsorbents was done for following purposes: 1) to verify the successful synthesis of allophanes; 2) to identify any co-precipitates, such as silicates (e.g. opal) or Al-hydroxides; 3) to characterize additional components within the natural allophane; and 4) to determine physicochemical and structural properties of the materials relevant for their adsorption behaviour.

5.1.1 Infrared Spectroscopy

Fourier transformation infrared (FTIR) spectroscopy sample technique using the attenuated total reflection (ATR) mode was carried out on a PerkinElmer FTIR Spectrometer 100 (Waltham, MA, USA) for qualitative and semi-qualitative analyses of functional groups in allophane. IR spectra of the natural and synthetic allophanes were compared with published allophanes spectra. The detection range was set in the mid infrared region (MIR) and yielded spectra from 4000 to 650 cm^{-1}; the spectra were scanned 4 times. Absorbance spectra were calculated from measured transmittance ones by using Equation (3), where A is the adsorbance and %T is the transmittance (as percentage).

$$A = 2 - log_{10}(\%T) \qquad (3)$$

5.1.2 X-ray Diffraction

For mineralogical characterization of the synthetic and natural allophanes, randomly oriented powder mounts were prepared by the top-loading technique in Al sample holders. X-ray powder diffraction patterns were recorded on a PANalytical X'Pert PRO diffractometer (Almelo, the Netherlands) using Co-K_α-radiation (wavelength λ = 0.179 nm). The devise was outfitted with a spinner stage, 0.5° antiscattering slit, 1° divergence slit, primary and secondary soller, and a high-speed Scientific X'Celerator detector. The machine was operated at X-ray tube operation conditions of 40 mA and 40 kV, in the 2θ range of 4 to 85° with step size of 0.008° and counting time of 40 s per step. The mineral phases were qualitatively analysed using the PANalytical High Score Plus software, version 3.0d (Almelo, the Netherlands), and ICSD database (provided by FIZ Karlsruhe).

[1]This chapter is published in *Geosciences*, **8**, 309: Baldermann et al. (2018).

5.1.3 Transmission Electron Microscopy

To determine the chemistry, nanostructure and shape of the allophane adsorbents, high-resolution imaging and energy dispersive X-ray spectroscopy (EDX) were performed on a FEI Tecnai F20 (FEI, Hillsboro, OR, USA) transmission electron microscopy (TEM) at the Institute of Electron Microscopy and Nanoanalysis at TU Graz (ZFE-FELMI). The device was operated at an accelerating voltage of 200 kV; the field emission gun was equipped with a monochromator (Schottky Field Emitter). An EDAX Saphire Si(Li) detector was used for the collection of EDX spectra. The analytical error for Si and Al analyses was determined to be ±2 at.% (Baldermann et al., 2018). The detection camera, equipped with an imaging filter (Gatan GIF Quantum with DualEELS for High-Speed Spectrum Imaging), and the analogue detection system (Gatan UltraScan CCD) provided high-resolution images with a TEM point resolution of 0.24 nm and TEM line resolution of 0.10 nm. Prior to the analyses, a dilute suspension of the allophane samples was deposited on a standard TEM copper grid (⌀ 3 mm), and dried under ambient air.

5.1.4 Specific Surface Area Measurements

Since surface area (SSA) is an important criterion in an adsorption process (i.e. greater surface area gives a higher adsorption capacity), the specific surfaces area of samples "n", "s1" and "s2" was analysed and used to normalize the obtained adsorption efficiency (% removal). Analysis was performed according to ISO 9277:2010 on a Micromeritics Flowsorb II 2300 (Micromeritics, Norcross/Georgia, USA) at the Institute of Technology and Testing of Construction Materials (IMBT) at TU Graz. The results were derived by enrichment of adsorptive gas (i.e. nitrogen) at the external and accessible internal surfaces of the powders. The Brunauer-Emmett-Teller (BET) method was used for data evaluation. Prior to the measurements, the samples were heated at 40 °C and 100 °C, respectively. Measurements were done at 25°C and under atmospheric pressure (967 mbar). Estimated analytical uncertainty is approx. ±10% (Baldermann et al., 2018).

5.2 Liquid Phase Characterization

5.2.1 pH, Temperature and Electrolytic Conductivity

The experimental solution pH and temperature (T) were measured using a SenTix 41 pH combination electrode (with gel electrolyte and integrated temperature sensor). Electric conductivity (EC) was measured at a reference temperature of 25 °C using a single-rod measuring cell with integrated temperature sensor. Both instruments were connected to a WTW Multi 3320 and/or a

[1]This chapter is published in *Geosciences*, **8**, 309: Baldermann et al. (2018).

WTW Terminal 740 (Zeller, Hohenems, Austria). Prior to measurements, the pH electrode was calibrated (three-point calibration using technical buffer solutions of pH 4.01, pH 7.00 and pH 10.01, from WTW, traceable to NIST), and the conductivity measuring cell was tested by use of a technical buffer solution. The analytical error of the pH measurements is ±0.05 pH units.

5.2.2 Inductively Coupled Plasma Optical Emission Spectrometry

Liquid samples collected from the allophane synthesis experiments (Chapter 4.1) and mainly from the kinetic and pH-drift experiments (Chapter 0 and Chapter 4.2.2) were analysed by inductively coupled plasma optical emission spectrometry (ICP-OES) using a PerkinElmer Optima 8300 (Waltham, MA, USA). The acidified samples (diluted to a 2% HNO_3 matrix) were analysed for their total concentrations of aqueous Ba, Co, Cr, Li, Sr and Zn (heavy metals); Al, Ca, Fe, Si and K (related to adsorbents); and Na (mainly related to the background electrolyte). The analytical precision (2σ, 3 replicates), reported relative to standard reference materials (NIST SRM 1640a and SPS-SW2 Batch 130), was determined as ±5% for Al, Ba, Ca, Fe, K, Na, Zn, and Si; ±3% for Cr and Sr; and ±0.1 for Li (Baldermann et al., 2018).

5.2.3 Hydrochemical Modelling with PHREEQC

Hydrochemical modelling (PHREEQC version 3.6.2, Lawrence Livermore National Laboratory (LLNL) database) of aqueous species of the metals Ba, Co, Sr, Zn, and Cr and of the saturation indices (SI) of the respective metal oxyhydroxides with respect to the experimental solutions was done at the experimental pH and temperature.

[1]This chapter is published in *Geosciences*, **8**, 309: Baldermann et al. (2018).

6. Results and Discussion

6.1 Characterization of Adsorbent Materials[1]

6.1.1 Mineralogy[1]

Infrared Data

IR spectra of synthetic ("s1", "s2") and natural ("n") allophanes are presented in Figure 5a (hydroxyl stretching region) and Figure 5b (lattice vibration region).

O-H stretching: The very broad IR band in the region **4000-2700 cm^{-1}** corresponds to stretching in hydroxyl groups and adsorbed H_2O, indicated as **ν(O-H)** and **ν(H-O-H)**). Very low intensity features in sample "n" are visible at ~3700 cm^{-1}, ~3625 cm^{-1}, ~3525 cm^{-1}, ~3450 cm^{-1}, ~3435 cm^{-1}, and ~3380 cm^{-1}, which are an indication for minor quantities of additional mineral phases. These are gibbsite and halloysite and / or kaolinite (Balan et al., 2006; Gates & Petit, 2017). The synthetic allophanes do not show such IR features.

H-O-H bending: The sharp **δ(H-O-H)** band is centred at **1639 cm^{-1}**, which indicates that all materials are hydrated. This feature is typical, but not exclusive, for hydrated aluminosilicates, such as allophane (Parfitt & Henmi, 1980).

Si-O stretching: In the region **1250-800 cm^{-1}**, the strongest IR bands appear for all adsorbents. For samples "s1" and "s2", the main signal, assigned to **ν(Si-O-Al),** appears as strong single band at 990 cm^{-1}, typical for pure allophane. By contrast, for sample "n", the **ν(Si-O-Al)** band appears as a doublet. The bands, which are assigned to allophane and silicate mineral impurities mentioned before, are centred at ~922 cm^{-1} (main band) and at ~996 cm^{-1}, respectively.

The position of the Si-O stretching vibration in silicates can be related to the polymerization degree of silicon in tetrahedral position (Parfitt & Henmi, 1980). Increasing polymerization of the tetrahedral network leads to stronger bonds and lower wavenumbers and vice versa. Since polymerization increases with increasing structural Si content, a shift to lower wavenumbers is also related to a higher Si(IV) content and accordingly a lower Al/Si ratio. Therefore, differences in wavenumbers for the Si-O stretch can be used to distinguish between allophane, imogolite, and their varieties. A doublet, as shown in "n", is often related to the tubular structure of imogolite (e.g. Levard et al., 2012), whereas a single IR band, as seen for the synthetic materials, is frequently related to allophane (e.g. Parfitt et al., 1980). However, IR spectra identical to that seen in sample "n" have been published for natural (Kaufhold et al., 2009) and synthetic allophanes (Iyoda et al., 2012; Rampe et al., 2010). Specifically, Kaufhold et al. (2009) have in-

[1]This chapter is published in *Geosciences*, **8**, 309: Baldermann et al. (2018).

vestigated the raw material ("PM-4-6") from the same location and depth, and concluded that the material is rich in allophane (Al/Si = 1.3±0.1, also confirmed by EDX point analyses). In case of samples "s1" and "s2", allophane with an Al/Si molar ratio of approximately 1 can be reasonably inferred from the IR data, which is in line with the synthesis protocol used. It can be concluded that sample "n" has a significantly higher Al/Si ratio compared to samples "s1" and "s2", in accordance with published literature (Iyoda et al., 2012; Levard et al., 2012).

In-plane Al-OH bending: Both synthetic materials show a distinct IR band at **~860 cm^{-1}**, attributed to **in-plane δ(Al-OH)** vibration in phyllosilicates (Bishop et al., 2013; Parfitt & Henmi, 1980) and to **Al(IV)-O** vibrations in synthetic allophane (Farmer et al., 1979; Rampe et al., 2010). The ~860 cm^{-1} band is indicative for Si-rich allophanes (Al/Si ratio of ~1) and also for silica-spring allophanes (Al/Si ratio of ~0.9-1.8), but it is not expected for imogolite or Al-rich allophane, which both show Al/Si molar ratios of ~2 (Farmer et al., 1979; Levard et al., 2012).

Out-of-plane Al-OH bending: Another IR band is observable for all three adsorbents at **~690 cm^{-1}**. Such a feature is generally only observed in phyllosilicates with a disrupted structure (e.g. Bishop & Murad, 2002). Regarding allophanes, the band is assigned to **Al(VI)-O** vibrations within alumina octahedral sheets (Farmer et al., 1979; Rampe et al., 2010) and it is originated from the peculiar wall structure of allophane (Iyoda et al., 2012; Parfitt, 1990).

Other IR bands, visible in sample "n" correspond to quartz (797 cm^{-1} and 788 cm^{-1}; Mu et al., 2014) and / or amorphous opal (small shoulder around 1200 cm^{-1}; Brown, 2005)). An IR band at ~742 cm^{-1} can be assigned to gibbsite (Balan et al., 2006). In the range between 755 and 753 cm^{-1}, IR bands typical for halloysite and kaolinite (Gates & Petit, 2017) are seen. Another weak IR signal in the region 1475-1415 cm^{-1} corresponds to the asymmetric stretching mode for CO_3 molecules (Weir & Lippincott, 1961), which are due to trace amounts of carbonates present in the sample.

[1]This chapter is published in *Geosciences*, **8**, 309: Baldermann et al. (2018).

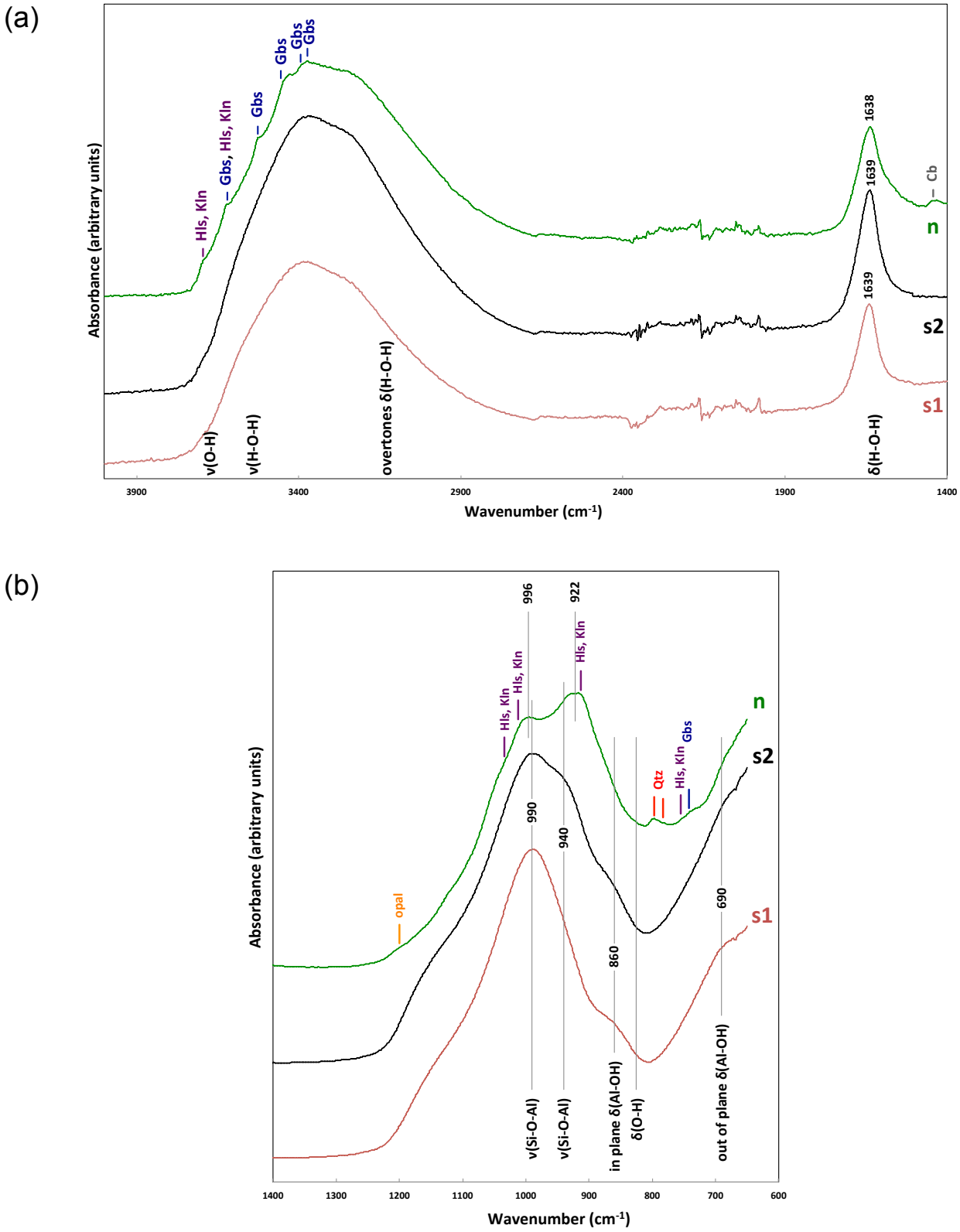

Figure 5. ATR-FTIR spectra for synthetic ("s1", "s2") and natural ("n") allophanes. Stretching vibrations are indicated by ν (Ny) and bending vibrations by δ (Delta). Vertical lines indicate positions of reference materials taken from published literature: Gbs = gibbsite (Balan et al., 2006)*, Hls = halloysite and Kln = kaolinite* (Gates & Petit, 2017)*, Qz = quartz* (Mu et al., 2014)*, Cb = carbonate minerals* (Weir & Lippincott, 1961) *and amorphous opal (Brown, 2005). For better visibility, spectra are shifted on the vertical scale.* ***(a)*** *Hydroxyl-stretching region (4000 to 1400 cm^{-1}). Spectra are shifted by absorbance of 0.01.* ***(b)*** *Lattice vibration region (1400 to 650 cm^{-1}). Spectra are shifted by absorbance of 0.05.*

[1]This chapter is published in *Geosciences*, **8**, 309: Baldermann et al. (2018).

XRD Data

Figure 6 presents the XRD patterns of samples "s1", "s2" and "n". In case of synthetic allophanes "s1" and "s2", the absence of well-defined peaks indicates the lack of long-range order possessing crystalline substances. However, two broad peaks are visible, implying a short-range ordered nature of the precipitated solids. The first peak, centred at ~30° 2θ (interatomic-spacing d = 3.4 Å), and the second peak, centred at ~47° 2θ (d = 2.3 Å), are both indicative for materials with an amorphous or nanocrystalline nature (Arakawa et al., 2014). They are typically observed for short-range ordered aluminosilicates, like allophane (i.e. Parfitt, 1990), corroborating the FTIR results. Besides, the co-precipitation of amorphous opal cannot be fully ruled out, because its peak positions overlie with allophane reflections. Apart from that both the purity and quality of the synthesised material meet the expectations, since no unwanted reaction by-products (at least in detectable amounts) are present in the synthetic materials. The natural allophane raw material ("n") (Figure 6) shows the same two diffraction peaks (~30° 2θ and ~47° 2θ) than the synthetic allophanes, confirming the predominance of allophane in this sample. Additional, sharp and intense peaks indicate the existence of minor amounts of crystalline substances in the material, such as quartz, cristobalite, hornblende, feldspar, goethite, gibbsite, and halloysite.

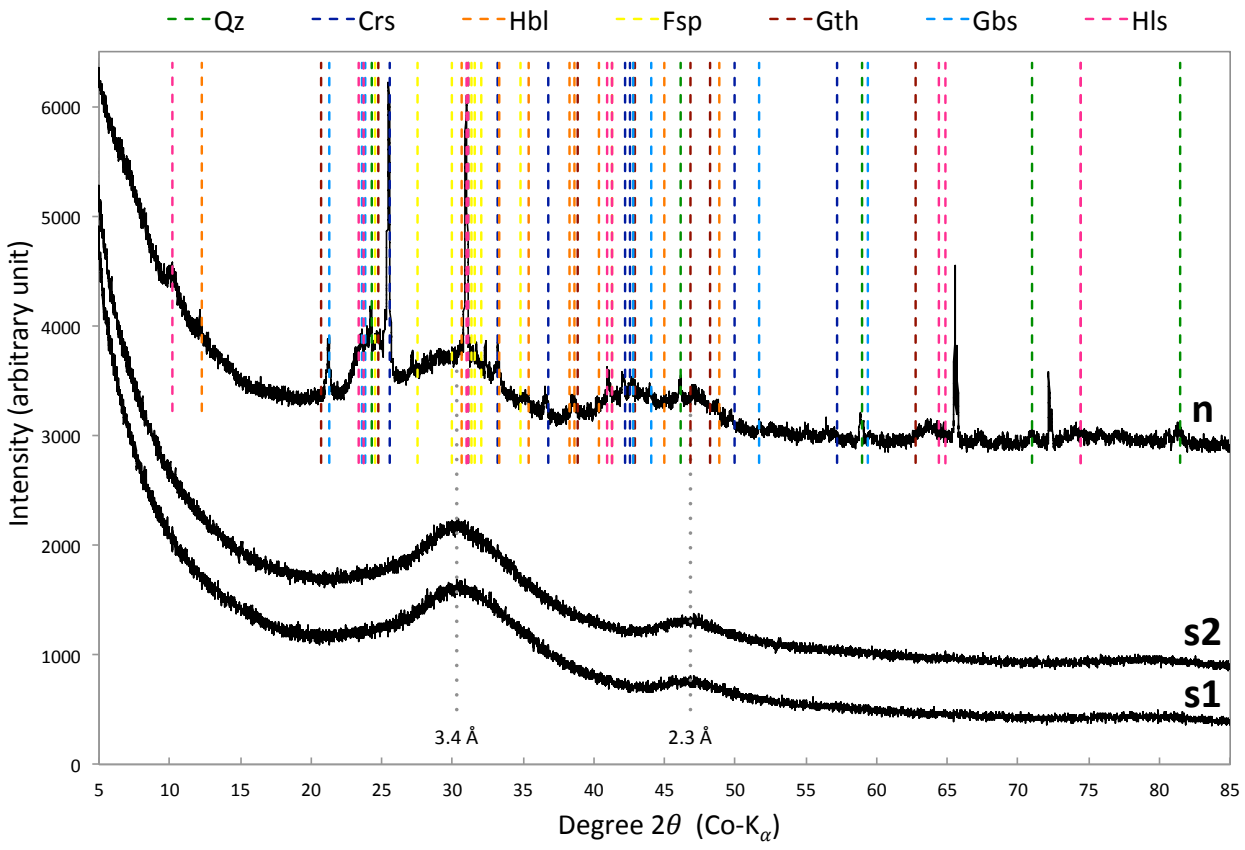

Figure 6. XRD patterns of synthetic allophanes ("s1" and "s2") and natural allophane raw material ("n"). Data are shifted on the y-axis for better comparability. The dotted lines (3.4 Å and 2.3 Å) mark the centre of the broad peaks that belong to allophane. Qz = quartz, Crs = cristobalite, Hbl = hornblende, Fsp = feldspar, Gth = goethite, Gbs = gibbsite, and Hls = halloysite.

[1]This chapter is published in *Geosciences*, **8**, 309: Baldermann et al. (2018).

6.1.2 Nanostructure, Particle Form and Chemical Composition[1]

TEM data

Transmission electron microscopy images (TEM) of synthetic ("s1" and "s2") and natural ("n") materials, shown in Figure 7 and Figure 8, reveal condensed (i.e. agglomerated) aggregates of allophane nano-particles. A closer inspection of the images shows that the aggregates are composed of rounded particles. These structures are related to allophane; i.e. they are described as ring-shaped and (in three dimension) may be composed of hollow spherules or polyhedrons (Henmi & Wada, 1976). Furthermore, in none of the three adsorbent materials, any evidence for the presence of tubular structures, related to imogolite (S.-I. Wada et al., 1979) is visible. As expected, the TEM images demonstrate the high purity of all three allophanes; in case of "s1" and "s2" they prove the successful synthesis of pure allophanes. All samples short-range order, i.e. lattice planes, is distorted across an individual allophane particle. In Figure 8, particles are highlighted and dimensioned for analysis of particle form and size. Regarding the aspect ratio, all allophanes have ratios about 1, which is typical for spherule particles. The average particle sizes of "s2" (x/y = 11/11 nm) are larger compared to those of "s1" (x/y = 6/5 nm) and "n" (x/y = 5/5 nm).

[1]This chapter is published in *Geosciences*, **8**, 309: Baldermann et al. (2018).

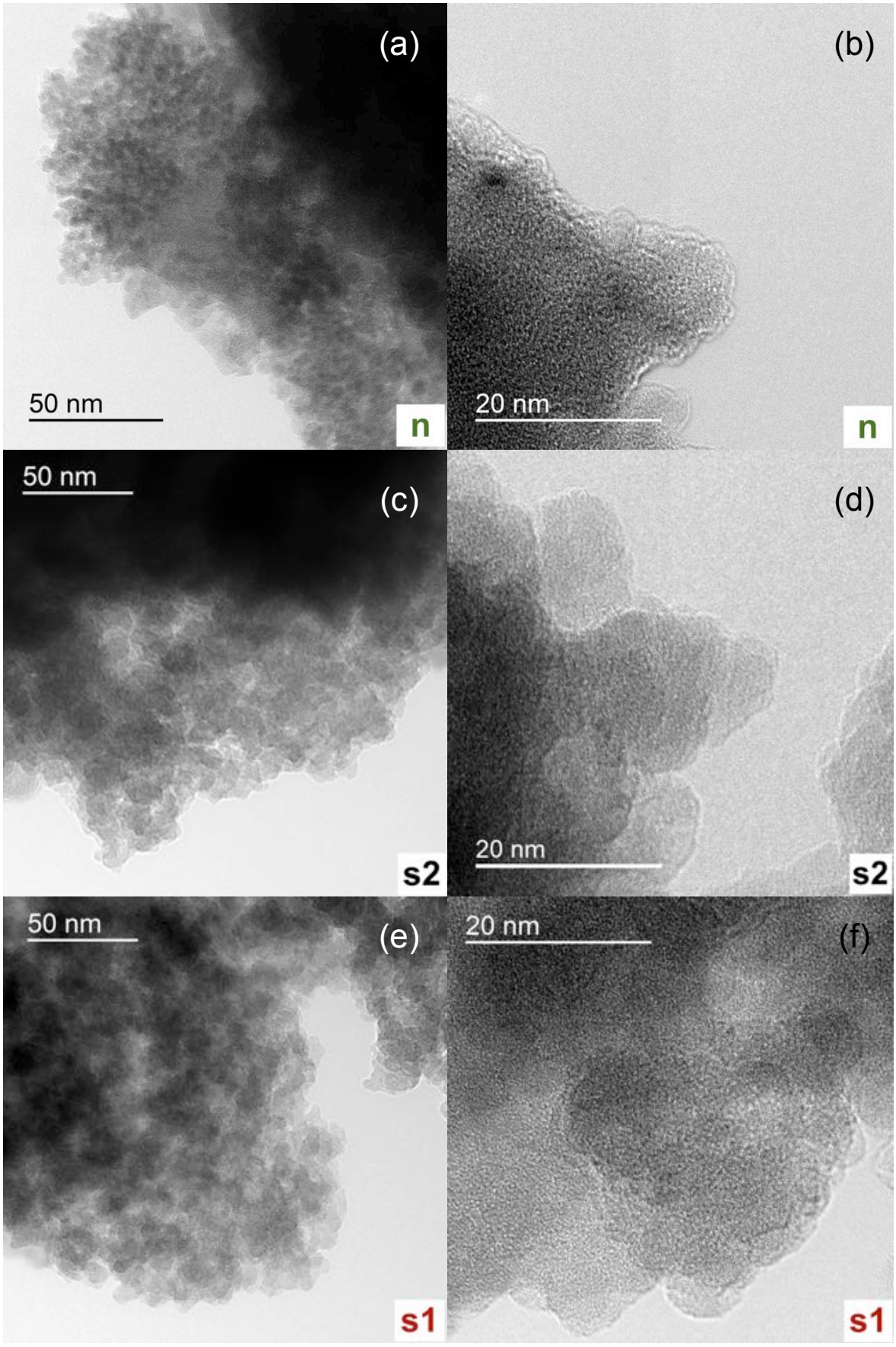

Figure 7. Transmission electron microscopy (TEM) images of allophane aggregates and particles. Note that images are shown at two different magnifications. ***(a), (b):*** *natural "n";* ***(c), (d):*** *synthetic "s2";* ***(e), (f):*** *synthetic "s1".*

[1]This chapter is published in *Geosciences*, **8**, 309: Baldermann et al. (2018).

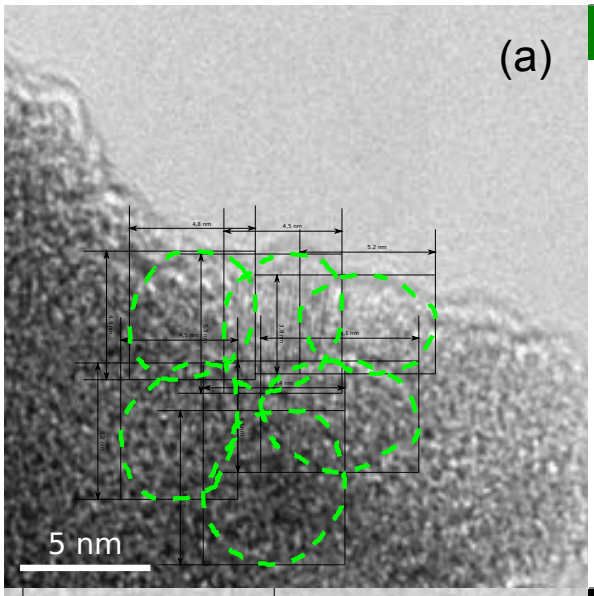

n	x	y	x/y
	4.8	4.9	1.0
	4.5	5.3	0.8
	5.2	3.8	1.4
	4.5	5.2	0.9
	5.4	5.9	0.9
	6.1	4.3	1.4

(b)

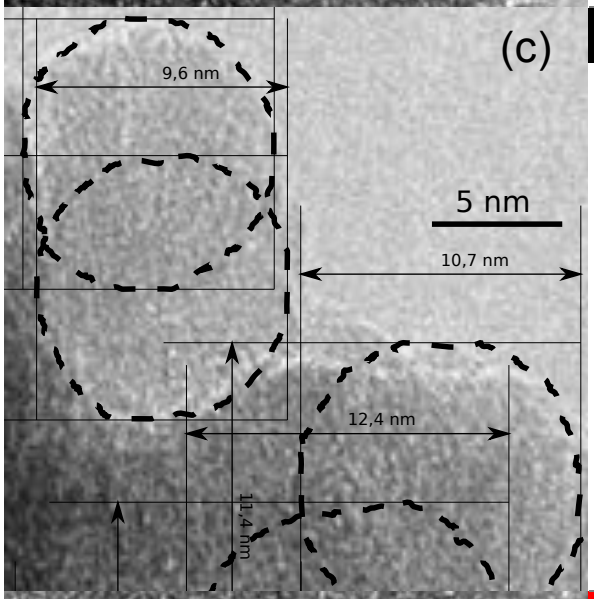

s2	x	y	x/y
	9.6	10.4	0.9
	9.6	10.1	1.0
	10.7	11.4	0.9
	12.4	11.8	1.1
	11	12.4	0.9
	11.2	11.9	0.9

(d)

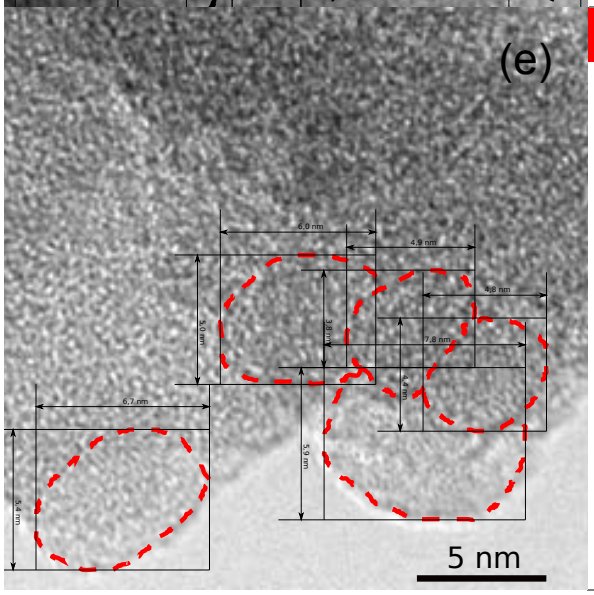

s1	x	y	x/y
	6.7	5.4	1.2
	6	5	1.2
	4.9	3.8	1.3
	4.8	4.4	1.1
	7.8	5.9	1.3

(f)

Figure 8. Selected sections of TEM images from Figure 3b, e and f, all magnified on the same scale and supplemented with particle size measurements (nm) and aspect ratios (x/y). ***(a), (b):*** *natural "n";* ***(c), (d):*** *synthetic "s2";* ***(e), (f):*** *synthetic "s1".*

[1]This chapter is published in *Geosciences*, **8**, 309: Baldermann et al. (2018).

EDX data

EDX (energy dispersive X-ray) spectroscopy provides qualitative and quantitative (considered as relative ratios) element analyses for the allophanes "s1", "s2" and "n". The resulting spectra (Figure 9) show oxygen (O), aluminium (Al), and silicon (Si) to be the most common elements in the samples. Hydrogen, also a main compound in allophane, is not displayed in EDX spectra since it gets lost under the electron beam. All of the spectra show peaks related to copper (Cu) and carbon (C); however, these elements are not supposed to originate from the samples. They are assigned to the copper grid and to the carbon support film, respectively. Similarly, iron (Fe) and cobalt (Co) come from the pole shoes in the microscope and are supposed to be a methodological/technical artefact. Only for sample "n", some of the Fe content possibly belongs to iron (hydr)oxides that are finely dispersed in the allophane matrix and on the allophane surfaces. In case of "s1" and "s2", an additional peak at 1.04 keV reveals minor amounts of sodium (Na), possibly due to traces of halite from synthesis. The Al/Si molar ratios were determined as 1.0 for "s1" and "s2", and 1.3 for "n" (Baldermann et al., 2018). Considering the Al/Si molar ratios, "s1" and "s2" are classified as Si-rich (in literature also called pumice or halloysite-like) allophanes, whereas "n" is associated with silica-spring (also called steam deposit or feldspathoid) allophanes (Levard et al., 2012; Parfitt, 1990).

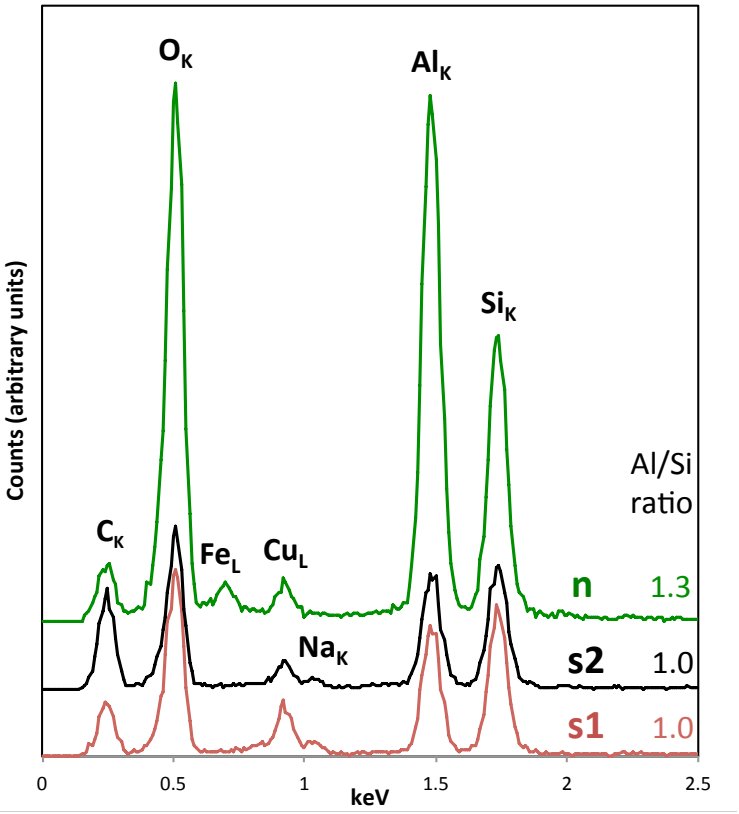

Figure 9. EDX spectra of synthetic ("s1" and "s2") and natural ("n") allophanes with qualitative assignments to elements (subscript indicates the orbital shell where the electrons de-excite). Peak areas are related to relative ratios of respective elements. Al/Si molar ratios of allophanes are provided on the right (Baldermann et al., 2018). For better visibility, spectra are shifted on the vertical scale.

[1]This chapter is published in *Geosciences*, **8**, 309: Baldermann et al. (2018).

6.1.3 Specific Surfaces Area[1]

BET data

Specific surface area (SSA) analyses by BET N_2 adsorption were carried out on materials dried at 40°C and at 100°C (for 24 h). **40°C:** Samples "n", "s1" and "s2" have SSAs of 205 m^2 / g, 290 m^2 / g and 282 m^2 / g, respectively. **100°C:** Samples "n", "s1" and "s2" have SSAs of 294 m^2 / g, 358 m^2 / g and 370 m^2 / g, respectively.

In natural state, structural micropores of allophanes are generally filled with water molecules that need to be removed for adsorption experiments; at the same time the structural integrity of the material needs to be maintained (Michot, 2018). The higher BET values observed for the allophanes dried at 100°C indicate that the temperature treatment at 40°C was not enough to sufficiently remove all water molecules sorbed on the allophanes. Thus, the results obtained at 100 °C pre-preparation will be used in the following. The specific surface area for "n" is in good agreement with previous results obtained for natural allophanes (Kaufhold et al., 2009). The higher values for "s1" and "s2" are in accordance with their higher purity; i.e. they are in the typical range for synthetic allophanes estimated by BET-N_2 adsorption (~300 m^2 / g to ~900 m^2 / g). Regarding the synthetic allophanes with Al/Si molar ratios of about 1, SSAs of ~400 m^2 / g (estimated by BET-method) have been reported (Iyoda et al., 2012; Kehal et al., 2011; Michot et al., 2005), which is qualitatively in line with the SSAs obtained here.

For allophanes, it has to be considered that by BET-N_2 method determined SSAs don't reveal the actual "total" SSAs. Allophanes are microporous materials (with pore width of 2 nm or less) and, hence, pores stay partly inaccessible to nitrogen; they don't contribute to the resulting SSAs (Michot, 2018; Paterson, 1977).

[1]This chapter is published in *Geosciences*, **8**, 309: Baldermann et al. (2018).

6.2 Adsorption Performance[1]

6.2.1 Thermodynamic Considerations[1]

Four PHREEQC simulations reproduce the four metal solutions at 25°C. The compositions are consistent with that of the pH-drift study (1 L solution containing each 10 mg of Ba^{2+}, Co^{2+}, Sr^{2+} and Zn^{2+}, respectively, and 10 mmol NaCl). Species distribution simulations are very useful to study adsorption processes within an aqueous environment. The specification (and charge) of an aqueous metal at a defined solution pH influence the adsorption mechanism, the site of adsorption and the amount of metal adsorbed on allophanes anisotropic distribution of charge on its inner and outer surfaces (Creton et al., 2008; Parfitt & Henmi, 1980; Preocanin et al., 2016; Su et al., 1992). To account for the metals that are influence by the solution pH, the aqueous specification is calculated over a range of pH values.

Aqueous Species Distribution: Figure 10 shows aqueous species distribution graphs for each metal solution as a function of pH. For better visibility of trends, the pH range for simulation is extended to the range of pH 4 to 10. **Barium solution:** The predominating species from pH 4.0 to 10.0 is Ba^{2+}. Further, minor quantities belong to $BaCl^{+}$ (<0.3%) and $BaOH^{+}$ (<0.05%). **Cobalt solution:** The most relevant species, Co^{2+} and $HCoO_2^{-}$, show both a clear dependency on pH. At pH 7.1, the concentrations of the two species are balanced. Co^{2+} is predominating at pH 4 to <7.1, whereas $HCoO_2^{-}$ dominates from pH >7.1 to 10. $CoCl^{+}$ (<1.3%) is present from pH 4.0 to 7.5. $Co(OH)_2$ occurs in minor quantity of <0.005%. Further species are present in negligible small quantities (<0.0001%). **Strontium solution:** Sr^{2+} is the predominating species from pH 4.0 to 10.0. Minor quantities belong to $SrCl^{+}$ (<0.4%) and $SrOH^{+}$ (<0.05%). **Zinc solution:** The most relevant species are Zn^{2+} and the uncharged species $Zn(OH)_2$, and both are strongly dependent on pH. The intersection of the two lines at pH 8.8 indicates balanced concentrations for the two species. Zn^{2+} is predominant below pH 8.8, whereas $Zn(OH)_2$ is dominant above. Also at pH 8.8, the two species $ZnOH^{+}$ and Zn(OH)Cl show highest amounts of 17.7% and 4.5% of the total aqueous Zn species, respectively. Under acid conditions, $ZnCl^{+}$ exists in small quantity (<1.4%), whereas $Zn(OH)_3^{-}$ occurs in the alkaline solution, where it increases to its maximum ratio (2.8%) at pH 9.9. Additional species occur in negligible small quantities (<0.05%).

[1]This chapter is published in *Geosciences*, **8**, 309: Baldermann et al. (2018).

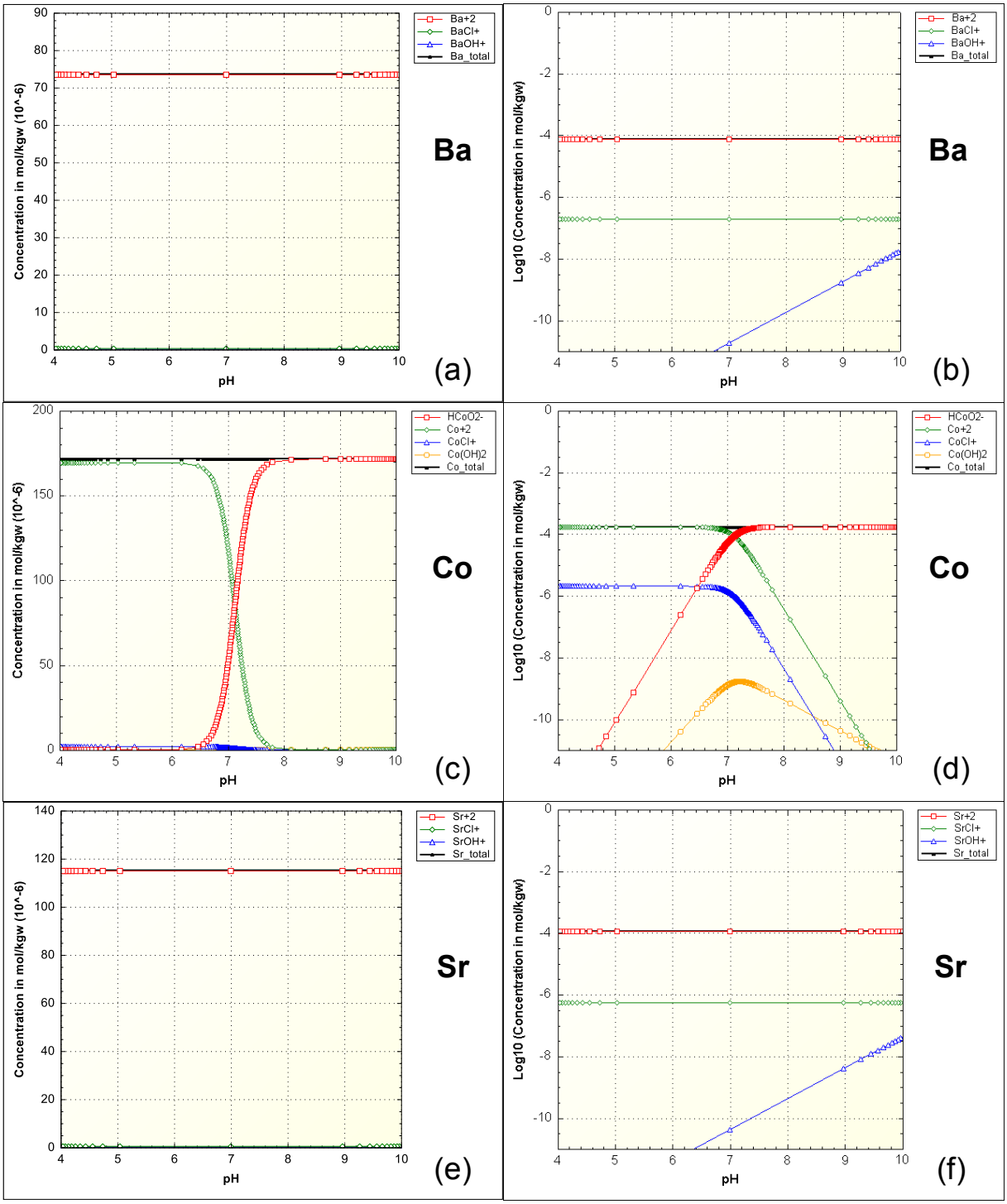

Figure 10. pH-drift study: Aqueous species distributions in the metal solutions used in the experiments plotted as a function of pH and established by PHREEQC. ***(a), (b):*** *Barium;* ***(c), (d):*** *Cobalt;* ***(e), (f):*** *Strontium;* ***(g), (h):*** *Zinc.*

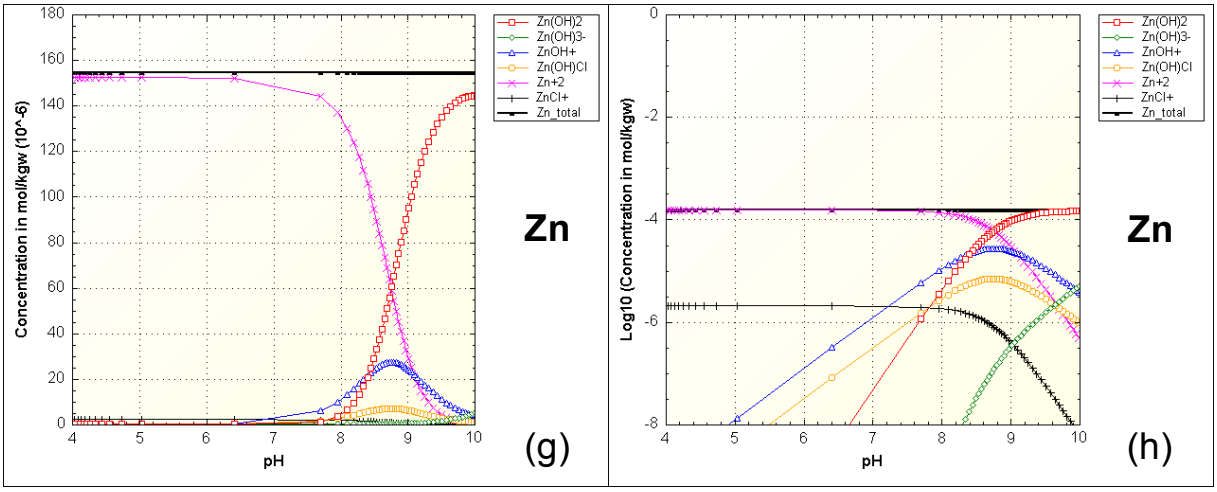

Figure 10. *Continued.*

Mineral Saturation: In the pH range from 4 to 10, the **metal solutions of Ba and Sr**, respectively, are all undersaturated with respect to any potential mineral phases containing these metal ions. Contrary, the **Co solution** is oversaturated with respect to spinel-Co (Co_3O_4). As visible in Figure 11a, spinel-Co is undersaturated from pH 4 to ~5.7, but is oversaturated afterwards, reaching the highest oversaturation at pH 7.0 to 7.5. At pH of ~9.9 spinel-Co is undersaturated again. As visible in Figure 11b, the **Zn solution** is partly oversaturated with respect to several Zn phases: Zincite (ZnO), $Zn(OH)_2$(beta), $Zn(OH)_2$(epsilon), $Zn(OH)_2$(gamma), and $Zn_2(OH)_3Cl$. Oversaturation of these phases occurs under alkalin conditions only, starting from pH 7.6 onwards.

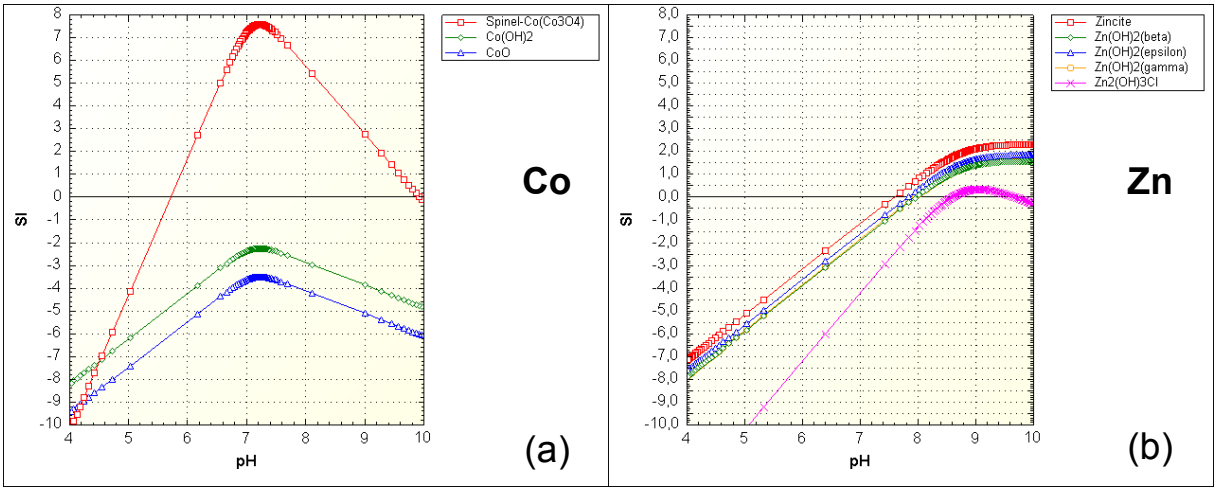

Figure 11. pH-drift study: metal solutions for ***(a):*** *Cobalt and* ***(b):*** *Zinc. Saturation indices of relevant phases are plotted as a function of pH.*

6.2.2 Kinetic Study[1]

The results of the kinetic study for the aqueous metals (Ba, Co, Sr, and Zn) are illustrated in Figure 12. The contact time (t, [min]) is plotted against the adsorption capacity at time t (q_t, [mg/g]), calculated by using Equation (1). For both pH conditions (pH 8.5 and 5.5, they are chosen to reflect the observed minima and maxima in adsorption from pH-drift experiments) the data reveal a high rate of adsorption within the first 5 min. After 5 min, a plateau is reached for Ba, Sr and Zn; the more or less constant q_t for the rest of the time indicates that an equilibrium between adsorption and desorption processes, defined as chemical steady-state between aqueous metal and allophane, is reached. Co needs more time to equilibrate; here a plateau is reached after 10 min. In general, the kinetic data reveal that a steady-state between adsorption and desorption processes between allophanes and the metal species is reached relatively fast. Within the first 10 min, equilibrium is achieved in all kinetic experiments, it indicates that all three allophanes are good candidates for metal ion uptake in aqueous environments. For all allophanes, the q_t values stay almost constant after achievement of steady-state for the whole run of experiment. That indicates that allophane is stabile within the pH conditions chosen in the experiments, that is also supposed by experimental data in publications that studied the stability of allophane (Wang et al., 2018, 2020). Electrostatic attraction is typically related to fast chemical reactions. By considering the distribution of charge on allophanes (Creton et al., 2008), discussed in Chapter 0 and the (under the chosen pH conditions) mainly positive charged aqueous metal species, highest attraction is supposed next to the passages or perforations that connect internal void and external space, and within the hollow structure of allophane. The process of uptake is most fast immediately after addition of allophane; that goes along with a high amount of vacant sites at the beginning and the gradually decrease of vacant sites by occupation of metal ions. In general, after 10 min the steady state between adsorption and desorption processes is achieved, and also the maximum of adsorption capacity for the respective solution pH is reached.

Table 4 lists equilibrium times in more detail, experimental data are supplemented by Pseudo-First-Order (PFO) parameters, that are achieved by the following equations after Lagergren (1898) and are recommended by Tran et al. (2017). Equation (4) shows the linear form of the PFO equation; q_e is calculated using equation (1), q_t is the amount of adsorbate uptake per mass of adsorbent at any time t (min) and k is the rate constant (1/min).

$$\ln(q_e - q_t) = -k \cdot t + \ln(q_e) \qquad (4)$$

[1]This chapter is published in *Geosciences*, **8**, 309: Baldermann et al. (2018).

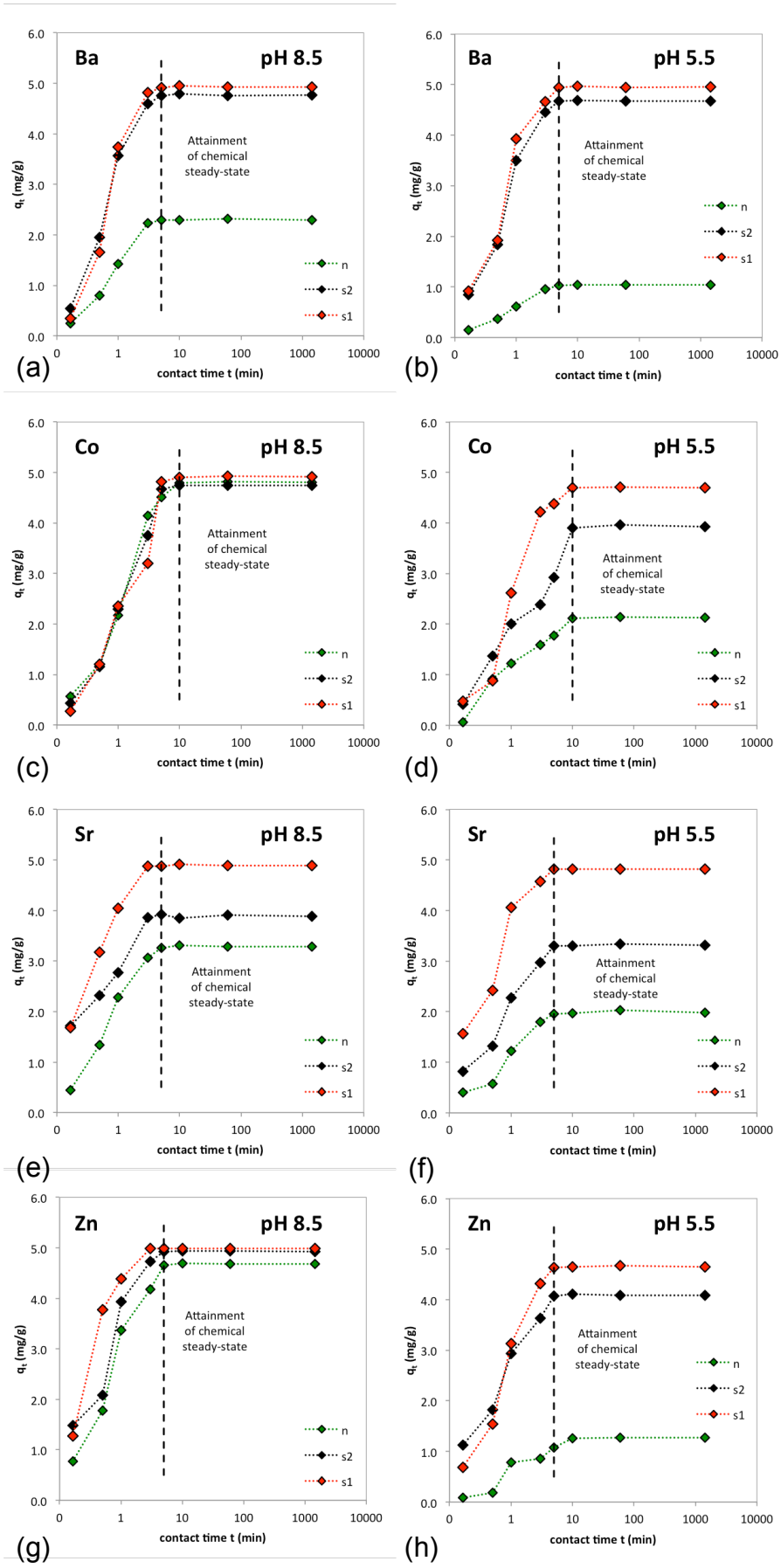

Figure 12. Effect of contact time on the adsorption behaviour of synthetic ("s1" and "s2") and natural ("n) allophanes, examined at constant pH 8.5 (left) and pH 5.5 (right), respectively. ***(a)***, ***(b)****: Barium;* ***(c)***, ***(d)****: Cobalt;* ***(e)***, ***(f)****: Strontium;* ***(g)***, ***(h)****: Zinc.*

[1]This chapter is published in *Geosciences*, **8**, 309: Baldermann et al. (2018).

Table 4. Outline of major predominating aqueous metal species at defined pH, required time to equilibriate measured adsorption capacity ($q_{e,exp}$) and %removal, all obtained from experimental data. Experimental data is supplemented by Pseudo-First-Order Parameters; since the plot of linear PFO equation reveals a linear trend, the parameters K, $q_{e,calc}$ and R^2 were determined by setting a trend line.

					Pseudo-First-Order Parameters			
					slope	offset		coeff. of determination
Adsorbent	**Adsorbate at pH 8.5**	**Equilibr. Time [min]**	**$q_{e,exp}$ [mg/g]**	**%removal [%]**	**K [1/min]**	**$\ln(q_{e,cal})$**	**$q_{e,cal}$ [mg/g]**	**R^2 [-]**
n	Ba^{2+}	5	2.3	45.2	1.090	0.9016	2.5	0.996
	$HCoO_2^-$	10	4.8	95.3	0.573	1.5157	4.6	0.988
	Sr^{2+}	5	3.3	65.8	0.948	1.1387	3.1	0.994
	Zn^{2+}	5	4.7	93.5	1.021	1.5889	4.9	0.953
s1	Ba^{2+}	5	4.9	97.0	1.179	1.5913	4.9	0.992
	$HCoO_2^-$	10	4.9	97.6	0.580	1.5908	4.9	0.942
	Sr^{2+}	3	4.9	97.9	2.003	1.6031	5.0	0.996
	Zn^{2+}	3	5.0	99.8	2.291	1.5981	4.9	0.996
s2	Ba^{2+}	5	4.8	93.9	1.150	1.5572	4.7	0.997
	$HCoO_2^-$	10	4.7	94.2	0.676	1.5745	4.8	0.977
	Sr^{2+}	3	3.9	77.8	1.667	1.3341	3.8	0.978
	Zn^{2+}	5	4.9	98.6	1.271	1.5679	4.8	0.977
Adsorbent	**Adsorbate at pH 5.5**	**Equilibr. Time [min]**	**q_e measured [mg/g]**	**%removal [%]**	**K [1/min]**	**$\ln(q_{e,cal})$**	**$q_{e,cal}$ [mg/g]**	**R^2 [-]**
n	Ba^{2+}	5	1.0	20.4	0.953	0.1267	1.1	0.989
	Co^{2+}	10	2.1	42.3	0.475	0.686	2.0	0.957
	Sr^{2+}	5	2.0	39.8	0.875	0.6899	2.0	0.994
	Zn^{2+}	10	1.3	25.3	0.462	0.244	1.3	0.965
s1	Ba^{2+}	5	4.9	97.4	1.134	1.5744	4.8	0.971
	Co^{2+}	10	4.7	93.3	0.635	1.5295	4.6	0.984
	Sr^{2+}	5	4.8	96.4	1.348	1.5236	4.6	0.942
	Zn^{2+}	5	4.7	93.0	0.986	1.5849	4.9	0.990
s2	Ba^{2+}	5	4.7	92.1	1.162	1.5714	4.8	0.986
	Co^{2+}	10	3.9	78.0	0.437	1.4168	4.1	0.925
	Sr^{2+}	5	3.3	66.4	1.046	1.255	3.5	0.952
	Zn^{2+}	5	4.1	81.7	1.014	1.3819	4.0	0.940

Plots of linear PFO equation for all tested aqueous metals and allophanes revealed that the experimental data follows a linear trend. The parameters K, $q_{e,calc}$ and R^2 were determined by setting a trend line for the respective data points.

The adsorption capacity (q_e) and the adsorption efficiency (%removal) are highest for allophane "s1"; that is valid for pH 8.5 (%removal >= 97.0%; $q_{e,exp}$ >= 4.9 mg/g) and pH 5.5 conditions (%removal >= 93.0%; $q_{e,exp}$ >= 4.7 mg/g), and true for each single aqueous metal. In this regard, "s1" is followed by "s2", that also shows go high values at pH 8.5 (%removal >= 77.8%; $q_{e,exp}$ >= 3.9 mg/g) and pH 5.5 (%removal >= 66.4%; $q_{e,exp}$ >= 3.3 mg/g). As expected, natural allophane "n" shows the lowest adsorption capacities and adsorption efficiencies for the tested aqueous metals. That can be contribute by a combination of factors (Chapter 6.1), that are e.g. lower purity compared with synthetic allophanes: "n" is a natural raw material with minor quantities of crystalline substances and**,** lower specific surface area determined by BET-N_2 method.

[1]This chapter is published in *Geosciences*, **8**, 309: Baldermann et al. (2018).

6.2.3 pH-drift Experiments[1]

In Figure 13, the adsorption performance of "s1, "s2" and "n" is expressed by two different parameters: as amount of adsorbate adsorbed at equilibrium q_e, and as the percentage of removed adsorbate from solution (%removal). However, the use of q_e is recommended whereas %removal is very approximate and should be used with caution (Tran et al., 2017).

Metal ion adsorption is well known to be pH dependent; regarding this it has to kept in mind that equilibrium data depend upon the equilibrium condition and not on the initial solution state (Tien, 2008). Adsorption studies that demonstrate the changes of the solution pH during the course of experiment are rare (Tien, 2008); the main focus of the present study was to yield data that account for that missing in experimental data. The reasons of allophanes pH-dependency are in detail discussed in Chapter 0. Depending on the pH of electrolytic solutions in contact, allophanes variable-charged surfaces, which are characterized by the presence of reactive functional groups, bear positive net charge in solutions below, and negative net charge in environments above the pH_{PZC} and pH_{PZNPC}. Figure 13 demonstrates how the pH influences the obtained adsorption performances of "s1", "s2" and "n". All allophanes show the same trend, the adsorption performance increases with higher pH values. Allophane "n" reveals the lowest performance in general, but "n" also shows the strongest influence by the pH value. Noticeable is here, that its performance in adsorbing Co is at higher pH (~8.5, %removal of ~96%) higher than that of "s2", and in case of Zn, "n" also performs very good at high pH (~7.5 – 8.5, %removal of ~90% to 94%); "n" is, hence, recommended to be used in this restricted pH range. A reason for "n" stronger dependency of adsorption performance on the pH can be a higher amount of more variable charged surface area on "n".

The adsorption performance of "s1" and "s2" is less variable at the different pH steps. Their adsorption behaviour is characterized by a good performance for the whole pH range ("s1": %removal of ~97% to 99%; "s2": %removal of ~80% to 95%). Hence, for "s1" and "s2" an application in a more varying pH environment can be contemplated. The best adsorption performance over all experiments shows "s1". The reasons why "s1" performs better than "s2" are not clear. Material characterization showed only small differences in BET surface areas between "s1" and "s2", areas of "s1" are smaller than that of "s2". More striking are the differences shown in the TEM images; the average particle sizes of "s1" (x/y= 6/5 nm) are significantly smaller than those of "s2" (x/y = 11/11 nm), consequential higher surface and, hence, more vacant sites can be a contribute to "s1" better performance.

Concentration of metal ions in solution and the effective radii of hydrated cations also contribute to the amount of physically adsorbed cations (Birrell, 1961). In hydrated state, the order of size has to be: Zn > Co > Sn > Ba. In the present data, no clear relation between effective radii and adsorption behaviour of the different aqueous metals can be found.

[1]This chapter is published in *Geosciences*, **8**, 309: Baldermann et al. (2018).

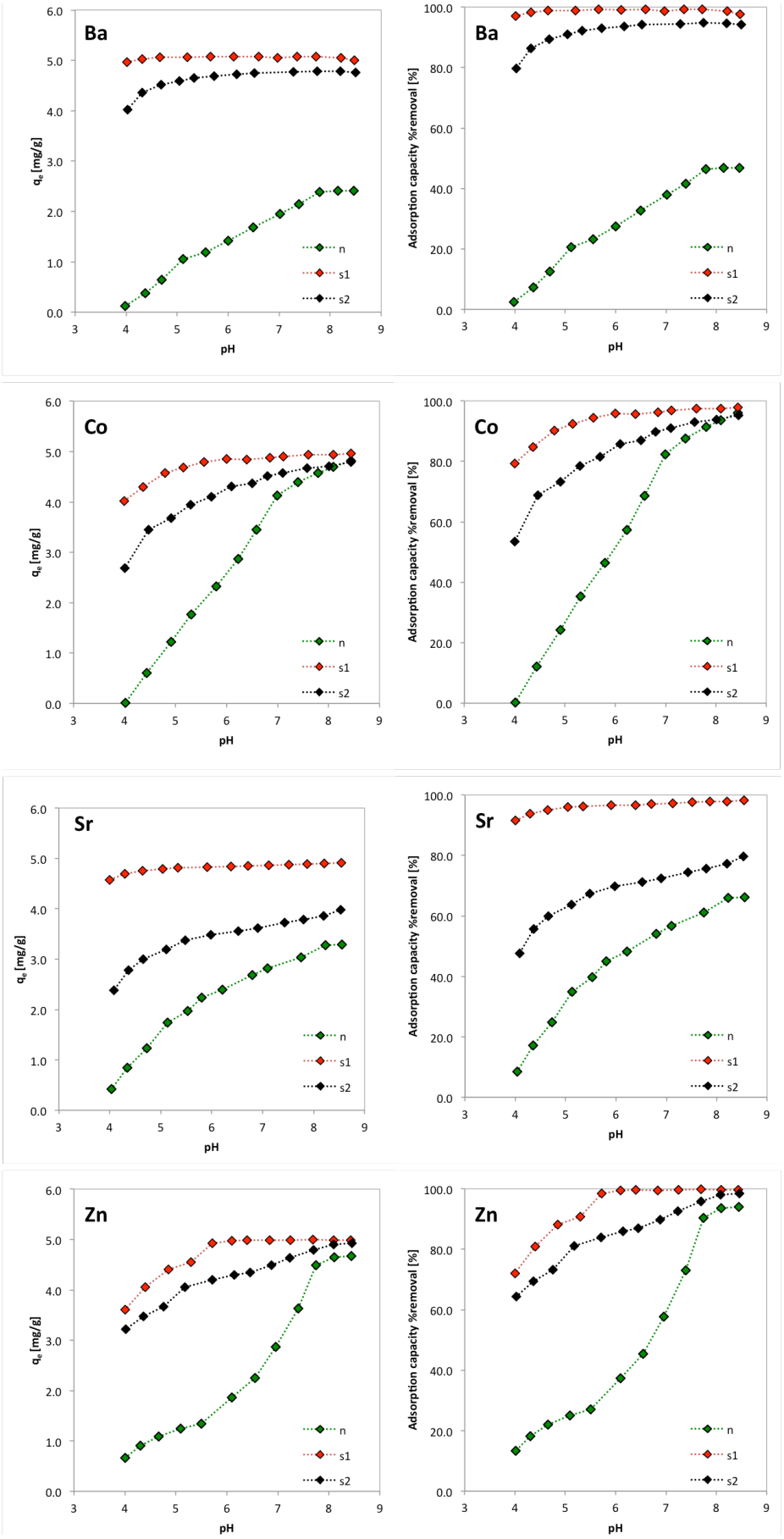

*Figure 13. Comparison of two different expression of adsorption performance, adsorption capacity q_e (**left column**) and adsorption efficiency %removal (**right column**) for the examined pH-drift.*

[1]This chapter is published in *Geosciences*, **8**, 309: Baldermann et al. (2018).

6.2.4 Allophane Adsorbents

On the one hand, the adsorption performance of allophane is ascribed to **allophanes characteristics** like its unique structure with high surface area and high reactivity as a consequence of its small particle size and hollow spheroidal morphology; external and internal surfaces which are characterized by the presence of abundant functional groups (e.g. Al-O,OH and [(O_3) Si(OH)]) that account for large adsorption capacity towards guest species (e.g. metal cations, anions, organic matter and water) in combination with defect sites (perforations) within the sphere walls, that additional to high reactive edge sites provide accessibility for water and small cations to the inner void (i.e. Parfitt, 1990; Theng et al., 1982). On the other hand, the adsorption behaviour of allophane is considerably depending on its hydration state and on the **pH and composition of the aqueous electrolyte solution** in contact.

In the text below, the structure of imogolite-type allophanes (Figure 14) is discussed, to those allophanes "s1" and "s2" belong to. They are characterized by the arrangement of functional aluminol (Al-OH) groups on their outer, and silanol (Si-OH) groups on the inner surface. It has to be considered that non-imogolite type allophanes, like allophane "n" is characterized as, clearly differ in structure and, hence, show a divergent arrangement of functional groups as described below (see Chapter 2.2 for details).

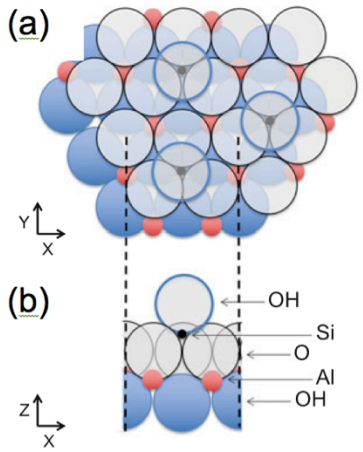

Figure 14. Imogolite-Local-Structure: (a) inner view from the inside of a unit particle model, (b) its side view (Nanzyo & Kanno, 2018)

Variable-charged Surfaces

Allophanes show **variable-charge (amphoteric) characteristics** that govern the adsorption of ions: controlled by the pH, the functional groups on the allophane outer surface can either be positively, negatively, or neutrally charged (Parfitt, 1990), established by protonation and deprotonation processes. The intrinsic property that characterises the electrical state of allophanes surface in electrolytic solutions is the pH at **point of zero charge (pH_{PZC})**. Nowadays, that

property is frequently more specifically termed as pH at **point of zero net proton charge (pH_{PZNPC})**. Both terms indicate the solutions pH under which the amphoteric surface is net uncharged subject to the definition (i.e. Appelo & Postma, 2005; Preocanin et al., 2016). Hence, allophanes variable charged surfaces bear positive net charge below, and negative net charge above the pH_{PZC} and pH_{PZNPC}, respectively. The predominance of H^+ in a more acidic solution may lead to proton adsorption and positive charge on the surface hydroxyl groups, whereas in more alkaline solutions, protons rather desorb and leave behind negative charged OH^-. For instance, the reactive $Al(OH)H_2O$ groups become $Al(OH_2)^+H_2O$ under acidic, and $Al(OH)(OH)^-$ under alkaline conditions (Parfitt, 1990). The surface charge of allophane and, accordingly, the values of pH_{PZC} and pH_{PZNPC}, depend on various factors like structural Al/Si molar ratio, structural charge due to substitutions, the ionic strength and the type and concentration of ions in the electrolyte solution, which form complexes at the surface (Appelo & Postma, 2005; Chunming & Harsh, 1993; Harsh et al., 1992). Hence, a wide range of different values for allophane can be found in literature. Especially, natural occurring allophanes are partly covered with complex forming ions which render the pH_{PZC} to lower values (Gustafsson et al., 1998). On allophanes variable charged surface sites, the driving mechanism of adsorption is electrostatic (Coulomb) force; it leads to the attraction of mobile anions and cations, from the adjacent aqueous medium (Birrell & Gradwell, 1956; K. Wada & Ataka, 1958). The **evolution of surface charges** is triggered by mutual reactions. Adsorptive processes influence the surface charges. By progressive covering of the surface, the number of vacant sites and the reactivity may decrease, or, by contrast, oppositional charge may arise by the attachment of ionic complexes that bare higher valences than needed for balanced charge. For instance, interaction of allophane with negative charged organic matter causes an increase in negative charge and, in case of positive charged surfaces, it decreases the positive charge (i.e. Parfitt, 1990; Perrott, 1978). And, furthermore, the ion load has to be consider: by the removal of ionic compounds from the aqueous electrolyte solution, the pH may react and change and, again, the pH will influences the charge of the amphoteric surfaces sites.

Distribution of surface charge: the electrostatic potential (EP) map in Figure 15 has been generated for a modelled allophane particle (Al-rich, imogolite-type) by Creton et al. (2008). Except for the difference, that the modelled allophane has no polymerized accessory Si attached to the tetrahedrons of the inner surface, the model is comparable with the allophanes "s1" and "s2" of the present study since both consist of an Imogolite-Local-structure (ILS). The EP map reveals an anisotropic distribution of the charge along the inner and outer surfaces. Several perforations (the 3-dimentional model contains six) connect the internal void with external space. Water molecules are able to enter the holes for an exchange between the "internal" and "external" water (Creton et al., 2008; Parfitt & Henmi, 1980). Anisotropy of charge is a behaviour which is also observed for the platelets of common clay minerals: those basal planes carry both, permanent and pH independent negative charges, whereas the edge faces show

amphoteric pH-dependency of charge which is similar to oxides (Preocanin et al., 2016). Indeed, the charging behaviour of allophane is more complex. In relation to the inside of its walls (EP = 0), the allophane in Figure 15 shows a slightly positive EP in the outer space and a negative potential inside of the structure. The passages are the most negative areas and it is noticeable that also the external space close to the holes is showing a negative potential (Creton et al., 2008).

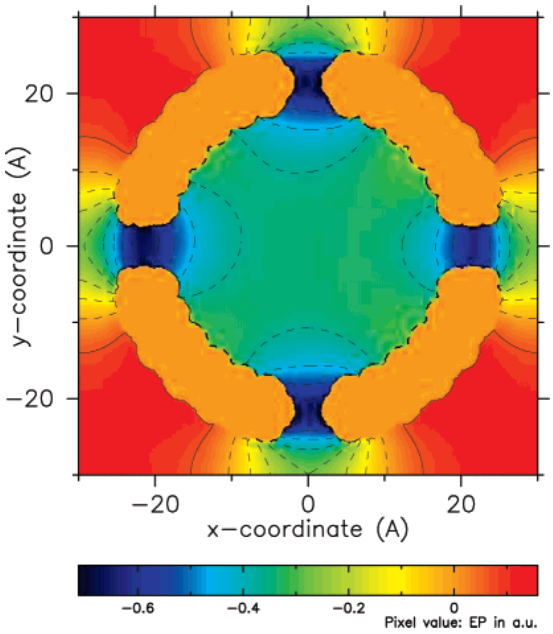

Figure 15. Electrostatic potential map for a modelled allophane (Al/Si ratio = 2.0; diameter: external 50 Å, internal 40 Å; with six perforations with ~7 Å size). EP values of inside of the allophane wall were arbitrarily set to 0 (Creton et al., 2008).

Permanent-charged Surfaces

Beside the more dominant amphoteric characteristics of allophanes, observations (PZNC vs. Point of zero salt effect, PZSE) imply the existence of permanent-charged surfaces that arise by isomorphic substitutions (Al^{3+} for Si^{4+} in tetrahedral position) imparting a permanent negative charge. And, although these surfaces are not expected to depend on proton concentration, they show effects by the salt concentration (and, hence, the ionic strength) of the adjacent solution by PZNC values that are lower than PZSE (Preocanin et al., 2016; Su et al., 1992).

Further Mechanism of Sorption/Adsorption

Beside of electrostatic attraction, **physical adsorption** in terms of pore filling is a mechanism which is strongly relevant for porous adsorbents (Tran et al., 2017) like allophane. The uptake of positively charged organic ions in parts of its pore space is experimentally proven (Parfitt, 1990; Theng, 1972).

Stability of Allophane in Aqueous Electrolyte Solutions

To evaluate allophanes applicability for industrial applications, knowledge about its behaviour and structural stability in varying aqueous environments is significant. The stability of allophane in aqueous solutions is effected by the pH (Wang et al., 2018, 2020). Under moderate alkaline conditions (pH ≤ 11.0), allophane particles show an almost intact structure, only slight dissolution of polymerized silicates appears but barely affect the framework of synthetic allophane; at pH > 11.0, enhanced dissolution of ILS leads to enlarged defect pores and, by implication, results in the collapse of allophanes hollow spherical structure (Wang et al., 2018). Under moderate acidic conditions (pH > 3.0), only slight dissolution of polymerized silicates appears and, thereby, increases the microporous parameters; at pH < 3.0, ILS dissolution enlarges defect pores or collapses the hollow spheres, which is followed by precipitation of amorphous silica and, thereby, more and more disordered products (Wang et al., 2020).

That implies a good stability of allophane under pH conditions found in most natural waters and, as well, for the pH range (pH 8.5 to 4.0) considered for the pH-drift experiments of this study.

7. Conclusions

Based on data from material characterization, thermodynamic considerations, literature research and the conductance of kinetic and equilibrium pH-drift experiments, links between metal ion adsorption performance and allophanes properties and structural features are elucidated.

The successful synthesis of allophane with an Al/Si molar ration of 1 ("s1" and "s2") was verified by a combination of analytical methods. All different characterization methods corroborated the successful syntheses of allophanes in expected high purity, quality and preferred molar Al/Si ratio. "s1" and "s2" (Al/Si molar ratios are 1) were classified as Si-rich allophanes, for "n" (Al/Si molar ratio = 1.3) the predominance of allophane was confirmed and it was associated with silica-spring allophanes. BET-method obtained specific surface areas (~ 364 m^2 / g for "s1" and "s2"; 294 m^2 / g for "n") in good accordance with data proposed in other studies for synthetic and natural allophanes, respectively. The kinetic studies provided equilibrium times to establish thermodynamic equilibrium between allophane and the representative aqueous metal ions of < 10 min. The high rate of adsorptive processes indicates that electrostatic attraction is a major adsorption mechanism in the conducted experiments. The adsorption of the aqueous Co in form of $HCoO_2^-$ at pH 8.5 demonstrated that allophane is also able to adsorb anions capacities comparable with that of adsorbed cations. All tested allophane materials have proven to be good candidates for an industrial application since they demonstrated high adsorption capacities, high rates of uptake and they are applicable as adsorbents under pH conditions of the most natural waters.

References

Abidin, Z., Matsue, N., & Henmi, T. (2013). ADSORPTION OF AMINES ON NANO-BALL ALLOPHANE AND ITS MOLECULAR ORBITAL ANALYSIS. *Clay Science*, *17*, 67–73.

Appelo, C. A. J., & Postma, D. (2005). *GEOCHEMISTRY, GROUNDWATER AND POLLUTION - SECOND EDITION*.

Arakawa, S., Matsuura, Y., & Okamoto, M. (2014). Allophane–Pt nanocomposite: Synthesis and MO simulation. *Applied Clay Science*, *95*, 191–196. https://doi.org/10.1016/j.clay.2014.04.012

Balan, E., Lazzeri, M., Morin, G., & Mauri, F. (2006). First-principles study of the OH-stretching modes of gibbsite. *American Mineralogist*, *91*(1), 115–119. https://doi.org/10.2138/am.2006.1922

Baldermann, A., Grießbacher, A. C., Baldermann, C., Purgstaller, B., Letofsky-Papst, I., Kaufhold, S., & Dietzel, M. (2018). Removal of Barium, Cobalt, Strontium, and Zinc from Solution by Natural and Synthetic Allophane Adsorbents. *Geosciences*, *8*(309). https://doi.org/10.3390/geosciences8090309

Barron, P. F., Wilson, M. A., Campbell, A. S., & Frost, R. L. (1982). Detection of imogolite in soils using solid state 29Si NMR. *Nature*, *299*(5884), 616–618. https://doi.org/10.1038/299616a0

Birrell, K. S. (1961). The adsorption of cations from solution by allophane in relation to their effective size. *Journal of Soil Sciencee*, *12*(2).

Birrell, K. S., & Gradwell, M. (1956). ION-EXCHANGE PHENOMENA IN SOME SOILS CONTAINING AMORPHOUS MINERAL CONSTITUENTS. *European Journal of Soil Science*, *69*, 2.

Bishop, J. L., & Murad, E. (2002). Spectroscopic and Geochemical Analyses of Ferrihydrite from Hydrothermal Springs in Iceland and Applications to Mars, in Volcano-Ice Interactions on Earth and Mars. *Geological Society, London, Special Publications*, *202*, 357–370.

Bishop, J. L., Rampe, E. B., Bish, D. L., Abidin, Z., Baker, L. L., Matsue, N., & Henmi, T. (2013). Spectral and Hydration Properties of Allophane and Imogolite. *Clays and Clay Minerals*, *61*, 57–74. https://doi.org/10.1346/CCMN.2013.0610105

Breithaupt, A. (1817). *Handbuch der Mineralogie von C.A.S. Hoffmann fortgesetzt von August*

Breithaupt (Vol. 4, pp. 181–182).

Breithaupt, A. (1829). *Jahrbuch der Chemie und Physik* (p. 306).

Brigatti, M. F., & Gala, E. (2013). Structure and Mineralogy of Clay Minerals. In *Handbook of Clay Science* (Vol. 5A, pp. 21–81). https://doi.org/10.1016/B978-0-08-098258-8.00002-X

Brigatti, M. F., Malferrari, D., Laurora, A., & Elmi, C. (2011). Structure and mineralogy of layer silicates : recent perspectives and new trends. In *EMU Notes in Mineralogy* (Vol. 11, pp. 1–71). https://doi.org/10.1180/EMU-notes.11.1

Brown, L. D. (2005). *Characterisation of Australian Opals - A thesis submitted for the award of Ph.D.* https://doi.org/10.13140/RG.2.2.27644.95360

Chevallier, T., Woignier, T., Toucet, J., Blanchart, E., & Dieudonné, P. (2008). Fractal structure in natural gels: Effect on carbon sequestration in volcanic soils. *Journal of Sol-Gel Science and Technology*, *48*(1–2), 231–238. https://doi.org/10.1007/s10971-008-1795-z

Childs, C. W., Parfitt, R. L., & Newman, R. H. (1990). Structural studies of Silica Springs allophane STUDIES OF SILICA SPRINGS. *Clay Minerals*, *25*, 329–341.

Chunming, S., & Harsh, J. B. (1993). The electrophoretic mobility of imogolite and allophane in the presence of inorganic anions and citrate. *Clays and Clay Minerals*, *41*(4), 461–471. https://doi.org/10.1346/CCMN.1993.0410407

Creton, B., Bougeard, D., Smirnov, K. S., Guilment, J., & Poncelet, O. (2008). Structural Model and Computer Modeling Study of Allophane. *The Journal of Physical Chemistry C*, *112*(2), 358–364. https://doi.org/10.1021/jp0738412

Elliott, S. R. (2001). Amorphous Materials: Medium-range Order. In K. H. J. Buschow, R. W. Cahn, M. C. Flemings, B. Ilschner, E. J. Kramer, S. Mahajan, & P. Veyssière (Eds.), *Encyclopedia of Materials: Science and Technology* (Vol. 1, pp. 215–219). Elsevier. https://doi.org/https://doi.org/10.1016/B0-08-043152-6/00046-2

Farmer, V. C., Fraser, A. R., & Tait, J. M. (1979). Characterization of the chemical structures of natural and synthetic aluminosilicate gels and sols by infrared spectroscopy. *Geochimica et Cosmochimica Acta*, *43*(9), 1417–1420. https://doi.org/10.1016/0016-7037(79)90135-2

Gates, W. P., & Petit, S. (2017). IR Spectra of Clay Minerals. In *Developments in Clay Science Volume 8 Infrared and Raman Spectroscopies of Clay Minerals* (Vol. 8). https://doi.org/10.1016/B978-0-08-100355-8.00005-9

Grathoff, G. H., Peterson, C. P., & Beckstrand, D. L. (2003). Coastal dune soils in Oregon, USA, forming allophane, imogolite and gibbsite. In E. Domínguez, G. Mas, & F. Cravero (Eds.), *2001. A Clay Odyssey* (1st Editio, pp. 197–203). Elsevier Science.

Gustafsson, J. P., Karltun, E., & Bhattacharya, P. (1998). *Allophane and imogolite in Swedish soils or why small , previously unknown , fibres influence the water quality in forests* (Issue September).

Harsh, J. B. (2005). AMORPHOUS MATERIALS. In D. B. T.-E. of S. in the E. Hillel (Ed.), *Encyclopedia of Soils in the Environment* (pp. 64–71). Elsevier. https://doi.org/10.1016/B0-12-348530-4/00207-1

Harsh, J. B., Traina, S. J., Boyle, J., & Yang, Y. (1992). ADSORPTION OF CATIONS ON IMOGOLITE AND THEIR EFFECT ON SURFACE CHARGE CHARACTERISTICS. *Clay and Clay Minerals*, *40*(6), 700–706.

Hashizume, H., & Theng, B. K. G. (2007). Adenine, adenosine, ribose and 5 ' -amp adsorption to allophane. *Clays and Clay Minerals*, *55*(6), 599–605. https://doi.org/10.1346/CCMN.2007.0550607

Hausmann, J. F. ., & Stromeyer, F. (1816). Über Silberkupferglanz und Allophan. *Göttingische Gelehrte Anzeigen*, *2*, 1251–1253.

Henmi, T., & Wada, K. (1976). Morphology and composition of allophane. *American Mineralogist*, *61*, 379–390. https://doi.org/not available

International Standard: ISO 9277:2010(E). (2010). *ISO*, *2*. https://doi.org/10.1016/j.jssc.2008.03.003

Iyoda, F., Hayashi, S., Arakawa, S., John, B., Okamoto, M., Hayashi, H., & Yuan, G. (2012). Synthesis and adsorption characteristics of hollow spherical allophane nano-particles. *Applied Clay Science*, *56*, 77–83. https://doi.org/10.1016/j.clay.2011.11.025

Kaufhold, S., Kaufhold, A., Jahn, R., Brito, S., Dohrmann, R., Hoffmann, R., Gliemann, H., Weidler, P., & Frechen, M. (2009). A new massive deposit of allophane raw material in Ecuador. *Clays and Clay Minerals*, *57*(1), 72–81. https://doi.org/10.1346/CCMN.2009.0570107

Kaufhold, S., Ufer, K., Kaufhold, A., Stucki, J. W., Anastácio, A. S., Jahn, R., & Dohrmann, R. (2010). Quantification of allophane from Ecuador. *Clays and Clay Minerals*, *58*(5), 707–716. https://doi.org/10.1346/ccmn.2010.0580509

Kehal, M., Ohashi, F., Goze-Bac, C., Duclaux, L., Bantignies, J.-L., & Reinert, L. (2011). Characterization and boron adsorption of hydrothermally synthesised allophanes. *Applied Clay Science*, *54*(3–4), 274–280. https://doi.org/10.1016/j.clay.2011.10.002

Lagergren, S. (1898). Zur theorie der sogenannten adsorption gelöster stoffe. *Kungliga Svenska Vetenskapsakademiens. Handlingar*, *24*(4), 1–39. https://doi.org/10.1007/BF01501332

Levard, C., & Basile-Doelsch, I. (2016). Geology and Mineralogy of Imogolite-Type Materials. In *Developments in Clay Science* (1st ed., Vol. 7, pp. 49–65). Elsevier Ltd. https://doi.org/10.1016/B978-0-08-100293-3.00003-0

Levard, C., Doelsch, E., Basile-Doelsch, I., Abidin, Z., Miche, H., Masion, A., Rose, J., Borschneck, D., & Bottero, J.-Y. (2012). Structure and distribution of allophanes, imogolite and proto-imogolite in volcanic soils. *Geoderma*, *183–184*, 100–108. https://doi.org/10.1016/j.geoderma.2012.03.015

Michot, L. J. (2018). Determination of surface areas and textural properties of clay minerals. In *Developments in Clay Science* (1st ed., Vol. 9, pp. 23–47). Elsevier Ltd. https://doi.org/10.1016/B978-0-08-102432-4.00002-0

Michot, L. J., Ghanbaja, J., Lartiges, B., Razafitianamaharavo, A., Montarges-Pelletier, E., Bogenez, S., & Pelletier, M. (2005). Synthetic allophane-like particles: textural properties. *Colloids and Surfaces A: Physicochemical and Engineering Aspects*, *255*(1–3), 1–10. https://doi.org/10.1016/j.colsurfa.2004.11.036

Mu, C. M., Pejcic, B., Esteban, L., Piane, C. D., Raven, M., & Mizaikoff, B. (2014). Infrared Attenuated Total Reflectance Spectroscopy : An Innovative Strategy for Analyzing Mineral Components in Energy Relevant Systems. *Scientific Reports*, 1–11. https://doi.org/10.1038/srep06764

Nanzyo, M., & Kanno, H. (2018). Non-crystalline Inorganic Constituents of Soil. In *Inorganic Constituents in Soil* (pp. 59–95). https://doi.org/10.1007/978-981-13-1214-4_4

Parfitt, R. L. (1990). Allophane in New Zealand-A Review. *Aust. J. Soil Res.*, *28*, 343–360. https://doi.org/10.1071/SR9900343

Parfitt, R. L., Furkert, R. J., & Henmi, T. (1980). Identification and Structure of Two Types of Allophane From Volcanic Ash Soils and Tephra. *Clays and Clay Minerals*, *28*(5), 328–334. http://www.clays.org/journal/archive/volume 28/28-5-328.pdf

Parfitt, R. L., & Henmi, T. (1980). Structure of Some Allophanes from New Zealand. *Clays and Clay Minerals, 28*(4), 285–294. https://doi.org/10.1346/CCMN.1980.0280407

Paterson, E. (1977). SPECIFIC SURFACE AREA AND PORE STRUCTURE OF ALLOPHANIC SOIL CLAYS. *Clay Minerals*, *12*(1), 1–9.

Perrott, K. W. (1978). The influence of organic matter extracted from humified clover on the properties of amorphous aluminosilicates. I. Surface charge. *Soil Research*, *16*(3), 327–339. https://doi.org/10.1071/SR9780327

Preocanin, T., Abdelmonem, A., Montavon, G., & Luetzenkirchen, J. (2016). Charging Behavior of Clays and Clay Minerals in Aqueous Electrolyte Solutions — Experimental Methods for Measuring the Charge and Interpreting the Results. *Clays, Clay Minerals and Ceramic Materials Based on Clay Minerals*, *March*. https://doi.org/10.5772/62082

Rampe, E. B., Christensen, P., Hervig, R., Shock, E., & Williams, L. (2011). *The Effects of Chemical Weathering on Thermal-Infrared Spectral Data and Models: Implications for Aqueous Processes on the Martian Surface*. ARIZONA STATE UNIVERSITY.

Rampe, E. B., Kraft, M. D., Sharp, T. G., Golden, D. C., & Ming, D. W. (2010). THERMAL INFRARED EMISSION SPECTROSCOPY OF SYNTHETIC ALLOPHANE AND ITS POTENTIAL FORMATION ON MARS. *Lunar and Planetary Science Conference (2010)*.

Ross, C. S., & Kerr, P. F. (1934). *Halloysite and allophane*.

Su, C., Harsh, J. B., & Bertsch, P. (1992). Sodium and Chloride Sorption by Imogolite and Allophanes1. *Clays and Clay Minerals*, *40*, 280–286. https://doi.org/10.1346/CCMN.1992.0400305

Theng, B. K. G. (1972). Adsorption of Ammonium and Some Primary n-Alkylammonium Cations by Soil Allophane. *Nature*, *238*(5360), 150–151. https://doi.org/10.1038/238150a0

Theng, B. K. G., Russel, M., Churchman, G. J., & Parfitt, R. L. (1982). Surface Properties of Allophane, Halloysite, and Imogolite. *Clays and Clay Minerals*, *30*(2), 143–149. https://doi.org/10.1346/ccmn.1982.0300209

Tien, C. (2008). Remarks on adsorption manuscripts revised and declined: An editorial. *Journal of Hazardous Materials*, *150*(1), 2–3. https://doi.org/https://doi.org/10.1016/j.jhazmat.2007.04.015

Tran, H. N., You, S. J., Hosseini-Bandegharaei, A., & Chao, H. P. (2017). Mistakes and inconsistencies regarding adsorption of contaminants from aqueous solutions: A critical review. *Water Research*, *120*, 88–116. https://doi.org/10.1016/j.watres.2017.04.014

UN-water. (2015). *Wastewater Management - A UN-Water Analytical Brief*.

https://doi.org/10.1016/j.jocs.2014.02.006

United Nations. (2009). *World Water Assessment Programme. 2009. The United Nations World Water Development Report 3: Water in a Changing World*. United Nations. https://doi.org/10.1142/9781848160682_0002

United Nations. (2017). *WWAP (United Nations World Water Assessment Programme). 2017. The United Nations World Water Development Report 2017: Wastewater, The Untapped Resource*. United Nations. https://unesdoc.unesco.org/ark:/48223/pf0000247153

von Leonhard, C. C. (1826). *Handbuch der Oryktognosie: für akademische Vorlesungen und zum Selbststudium* (Vol. 2, pp. 183–185).

Wada, K. (1978). Chapter 4 Allophane and imogolite. In T. Sudo & S. B. T.-D. in S. Shimoda (Eds.), *Clays and Clay Minerals of Japan* (Vol. 26, pp. 147–187). Elsevier. https://doi.org/https://doi.org/10.1016/S0070-4571(08)70685-X

Wada, K., & Ataka, H. (1958). The ion uptake mechanism of allophane. *Soil and Plant Food*, *4*(1), 12–18. https://doi.org/10.1080/00380768.1958.10431933

Wada, S.-I., Eto, A., & Wada, K. (1979). Synthetic Allophane and Imogolite. *Journal of Soil Science*, *30*, 347–355. https://doi.org/10.1111/j.1365-2389.1979.tb00991.x

Wada, S.-I., & Wada, K. (1977). Density and structure of allophane. *Clay Minerals*, *12*, 289–298.

Wang, S., Du, P., Yuan, P., Zhong, X., Liu, Y., & Liu, D. (2018). Applied Clay Science Changes in the structure and porosity of hollow spherical allophane under alkaline conditions. *Applied Clay Science*, *166*(October), 242–249. https://doi.org/10.1016/j.clay.2018.09.028

Wang, S., Yuan, P., Du, P., Liu, Y., & Liu, D. (2020, June 8). *Acid-induced alterations of the structure of allophane*.

Weir, C. E., & Lippincott, E. R. (1961). Infrared Studies of Aragonite , Calcite , and Vaterite Type Structures in the Borates , Carbonates , and Nitrates. *Journal of Research of the National Bureau of Standards - A. Physics and Chemistry*, *65*(3), 173–183.

Yuan, G., & Wada, S.-I. (2012). Allophane and imogolite nanoparticles in soil and their environmental applications. *Nature's Nanostructures*, *8*, 493–516. https://doi.org/10.1201/b11618-24

Appendix

A- 1 Raw data from kinetic study at pH 8.5

n	pH 8.5			pH 8.5			pH 8.5			pH 8.5		
(min)	Ba (µg/L)	ci/c0	qe	Co (µg/L)	ci/c0	qe	Sr (µg/L)	ci/c0	qe	Zn (µg/L)	ci/c0	qe
0	10160	1.00	0.00	10077	1.00	0.00	9989	1.00	0.00	10003	1.00	0.00
0.2	9667	0.95	0.25	8934	0.89	0.57	9090	0.91	0.45	8446	0.84	0.78
0.5	8569	0.84	0.80	7678	0.76	1.20	7312	0.73	1.34	6456	0.65	1.77
1	7323	0.72	1.42	5745	0.57	2.17	5424	0.54	2.28	3252	0.33	3.38
3	5707	0.56	2.23	1783	0.18	4.15	3856	0.39	3.07	1634	0.16	4.18
5	5584	0.55	2.29	1062	0.11	4.51	3459	0.35	3.27	683	0.07	4.66
10	5578	0.55	2.29	487	0.05	4.80	3378	0.34	3.31	612	0.06	4.70
60	5528	0.54	2.32	452	0.04	4.81	3412	0.34	3.29	652	0.07	4.68
1440	5563	0.55	2.30	470	0.05	4.80	3416	0.34	3.29	649	0.06	4.68
s1	Ba (µg/L)	ci/c0	qe	Co (µg/L)	ci/c0	qe	Sr (µg/L)	ci/c0	qe	Zn (µg/L)	ci/c0	qe
0	10160	1.00	0.00	10077	1.00	0.00	9989	1.00	0.00	10003	1.00	0.00
0.2	9467	0.93	0.35	9525	0.95	0.28	6628	0.66	1.68	7456	0.75	1.27
0.5	6838	0.67	1.66	7660	0.76	1.21	3629	0.36	3.18	2457	0.25	3.77
1	2675	0.26	3.74	5373	0.53	2.35	1892	0.19	4.05	1225	0.12	4.39
3	525	0.05	4.82	3687	0.37	3.20	232	0.02	4.88	33	0.00	4.99
5	332	0.03	4.91	445	0.04	4.82	224	0.02	4.88	17	0.00	4.99
10	267	0.03	4.95	276	0.03	4.90	156	0.02	4.92	20	0.00	4.99
60	301	0.03	4.93	213	0.02	4.93	212	0.02	4.89	25	0.00	4.99
1440	300	0.03	4.93	245	0.02	4.92	206	0.02	4.89	24	0.00	4.99
s2	Ba (µg/L)	ci/c0	qe	Co (µg/L)	ci/c0	qe	Sr (µg/L)	ci/c0	qe	Zn (µg/L)	ci/c0	qe
0	10160	1.00	0.00	10077	1.00	0.00	9989	1.00	0.00	10003	1.00	0.00
0.2	9076	0.89	0.54	9223	0.92	0.43	6564	0.66	1.71	7045	0.70	1.48
0.5	6265	0.62	1.95	7769	0.77	1.15	5365	0.54	2.31	5846	0.58	2.08
1	3035	0.30	3.56	5479	0.54	2.30	4456	0.45	2.77	2123	0.21	3.94
3	963	0.09	4.60	2578	0.26	3.75	2254	0.23	3.87	544	0.05	4.73
5	649	0.06	4.76	738	0.07	4.67	2143	0.21	3.92	155	0.02	4.92
10	572	0.06	4.79	591	0.06	4.74	2284	0.23	3.85	127	0.01	4.94
60	645	0.06	4.76	578	0.06	4.75	2170	0.22	3.91	136	0.01	4.93
1440	622	0.06	4.77	585	0.06	4.75	2213	0.22	3.89	139	0.01	4.93

A- 2 Raw data from kinetic study at pH 5.5

n	pH 5.5			pH 5.5			pH 5.5			pH 5.5		
(min)	Ba (µg/L)	ci/c0	qe	Co (µg/L)	ci/c0	qe	Sr (µg/L)	ci/c0	qe	Zn (µg/L)	ci/c0	qe
0	10160	1.00	0.00	10077	1.00	0.00	9989	1.00	0.00	10003	1.00	0.00
0.2	9861	0.97	0.15	9946	0.99	0.07	9190	0.92	0.40	9834	0.98	0.08
0.5	9434	0.93	0.36	8242	0.82	0.92	8846	0.89	0.57	9648	0.96	0.18
1	8936	0.88	0.61	7623	0.76	1.23	7534	0.75	1.23	8432	0.84	0.79
3	8263	0.81	0.95	6890	0.68	1.59	6383	0.64	1.80	8289	0.83	0.86
5	8096	0.80	1.03	6530	0.65	1.77	6074	0.61	1.96	7843	0.78	1.08
10	8078	0.80	1.04	5842	0.58	2.12	6051	0.61	1.97	7483	0.75	1.26
60	8085	0.80	1.04	5790	0.57	2.14	5923	0.59	2.03	7452	0.74	1.28
1440	8086	0.80	1.04	5816	0.58	2.13	6016	0.60	1.99	7467.5	0.75	1.27
s1	Ba (µg/L)	ci/c0	qe	Co (µg/L)	ci/c0	qe	Sr (µg/L)	ci/c0	qe	Zn (µg/L)	ci/c0	qe
0	10160	1.00	0.00	10077	1.00	0.00	9989	1.00	0.00	10003	1.00	0.00
0.2	8318	0.82	0.92	9121	0.91	0.48	6856	0.69	1.57	8625	0.86	0.69
0.5	6319	0.62	1.92	8322	0.83	0.88	5157	0.52	2.42	6926	0.69	1.54
1	2294	0.23	3.93	4846	0.48	2.62	1858	0.19	4.07	3737	0.37	3.13
3	845	0.08	4.66	1634	0.16	4.22	851	0.09	4.57	1363	0.14	4.32
5	285	0.03	4.94	1323	0.13	4.38	355	0.04	4.82	723	0.07	4.64
10	237	0.02	4.96	691	0.07	4.69	362	0.04	4.81	712	0.07	4.65
60	264	0.03	4.95	668	0.07	4.70	359	0.04	4.82	656	0.07	4.67
1440	262	0.03	4.95	680	0.07	4.70	359	0.04	4.82	697	0.07	4.65
s2	Ba (µg/L)	ci/c0	qe	Co (µg/L)	ci/c0	qe	Sr (µg/L)	ci/c0	qe	Zn (µg/L)	ci/c0	qe
0	10160	1.00	0.00	10077	1.00	0.00	9989	1.00	0.00	10003	1.00	0.00
0.2	8479	0.83	0.84	9247	0.92	0.42	8341	0.84	0.82	7753	0.78	1.13
0.5	6480	0.64	1.84	7348	0.73	1.36	7342	0.74	1.32	6354	0.64	1.82
1	3152	0.31	3.50	6062	0.60	2.01	5446	0.55	2.27	4124	0.41	2.94
3	1263	0.12	4.45	5313	0.53	2.38	4036	0.40	2.98	2745	0.27	3.63
5	823	0.08	4.67	4242	0.42	2.92	3373	0.34	3.31	1854	0.19	4.07
10	789	0.08	4.69	2284	0.23	3.90	3389	0.34	3.30	1794	0.18	4.10
60	801	0.08	4.68	2156	0.21	3.96	3301	0.33	3.34	1832	0.18	4.09
1440	804	0.08	4.68	2220	0.22	3.93	3354	0.34	3.32	1827	0.18	4.09

A- 3 Raw data from pH-drift Experiment, Barium and Cobalt

Ba_n	Ba-n-St	Ba-n-Eq	Ba-n-1	Ba-n-2	Ba-n-3	Ba-n-4	Ba-n-5	Ba-n-6	Ba-n-7	Ba-n-8	Ba-n-9	Ba-n-10	Ba-n-11
Conc. [µg/L]	10285	5469	5461	5503	6004	6381	6925	7458	7900	8170	9002	9532	10046
pH	5.93	8.46	8.15	7.80	7.39	7.02	6.49	6.00	5.56	5.12	4.70	4.37	3.98
q_e		2.4	2.4	2.4	2.1	2.0	1.7	1.4	1.2	1.1	0.6	0.4	0.1
%removal		46.8	46.9	46.5	41.6	38.0	32.7	27.5	23.2	20.6	12.5	7.3	2.3

Ba_s1	Ba-S1-St	Ba-S1-Eq	Ba-S1-1	Ba-S1-2	Ba-S1-3	Ba-S1-4	Ba-S1-5	Ba-S1-6	Ba-S1-7	Ba-S1-8	Ba-S1-9	Ba-S1-10	Ba-S1-11
Conc. µg/L	10229	234	141	78	75	138	84	86	83	111	112	178	295
pH	5.93	8.48	8.22	7.72	7.36	6.97	6.60	6.11	5.66	5.20	4.66	4.31	4.01
q_e		5.0	5.0	5.1	5.1	5.0	5.1	5.1	5.1	5.1	5.1	5.0	5.0
%removal		97.7	98.6	99.2	99.3	98.7	99.2	99.2	99.2	98.9	98.9	98.3	97.1

Ba_s2	Ba-S2-St	Ba-S2-Eq	Ba-S2-1	Ba-S2-2	Ba-S2-3	Ba-S2-4	Ba-S2-5	Ba-S2-6	Ba-S2-7	Ba-S2-8	Ba-S2-9	Ba-S2-10	Ba-S2-11
	< 1	< 1	< 1	< 1	< 1	< 1	< 1	< 1	< 1	< 1	< 1	< 1	14
Conc. µg/L	10095	579	536	529	559	592	646	713	797	904	1072	1377	2045
pH	5.93	8.50	8.21	7.75	7.28	6.52	6.17	5.72	5.34	5.05	4.68	4.32	4.03
q_e		4.8	4.8	4.8	4.8	4.8	4.7	4.7	4.6	4.6	4.5	4.4	4.0
%removal		94.3	94.7	94.8	94.5	94.1	93.6	92.9	92.1	91.0	89.4	86.4	79.7

Co_n	Co_n_st	Co_n_eq	Co_n_1	Co_n_2	Co_n_3	Co_n_4	Co_n_5	Co_n_6	Co_n_7	Co_n_8	Co_n_9	Co_n_10	Co_n_11
Conc. [µg/L]	10033	391	641	872	1252	1773	3143	4284	5379	6498	7594	8812	10009
pH	6.40	8.44	8.10	7.80	7.40	7.00	6.58	6.23	5.80	5.31	4.91	4.44	4.01
q_e		4.8	4.7	4.6	4.4	4.1	3.4	2.9	2.3	1.8	1.2	0.6	0.0
%removal		96.1	93.6	91.3	87.5	82.3	68.7	57.3	46.4	35.2	24.3	12.2	0.2

Co_s1	Co_s1_st	Co_s1_eq	Co_s1_1	Co_s1_2	Co_s1_3	Co_s1_4	Co_s1_5	Co_s1_6	Co_s1_7	Co_s1_8	Co_s1_9	Co_s1_10	Co_s1_11
Conc. [µg/L]	10139	225	256	252	330	378	444	428	562	767	990	1538	2101
pH		8.44	8.10	7.61	7.12	6.85	6.40	6.00	5.57	5.16	4.79	4.36	4.00
q_e		5.0	4.9	4.9	4.9	4.9	4.8	4.9	4.8	4.7	4.6	4.3	4.0
%removal		97.8	97.5	97.5	96.7	96.3	95.6	95.8	94.5	92.4	90.2	84.8	79.3

Co_s2	Co_s2_st	Co_s2_eq	Co_S2_1	Co_S2_2	Co_S2_3	Co_S2_4	Co_S2_5	Co_S2_6	Co_S2_7	Co_S2_8	Co_S2_9	Co_S2_10	Co_S2_11
Conc. [µg/L]	10053	474	628	703	907	1032	1317	1426	1851	2157	2687	3142	4679
pH		8.44	8.01	7.58	7.10	6.80	6.50	6.10	5.70	5.30	4.92	4.47	4.00
q_e		4.8	4.7	4.7	4.6	4.5	4.4	4.3	4.1	3.9	3.7	3.5	2.7
%removal		95.3	93.8	93.0	91.0	89.7	86.9	85.8	81.6	78.5	73.3	68.7	53.5

A- 4 Raw data from pH-drift Experiment, Strontium and Zinc

Sr_n	Sr-n-st	Sr-n-eq	Sr-n-1	Sr-n-2	Sr-n-3	Sr-n-4	Sr-n-5	Sr-n-6	Sr-n-7	Sr-n-8	Sr-n-9	Sr-n-10	Sr-n-11	
Conc. [µg/L]	9937	3359	3381	3871	4307	4557	5142	5461	5994	6467	7474	8238	9102	
pH	8.33	8.56	8.23	7.75	7.10	6.80	6.21	5.80	5.52	5.13	4.73	4.35	4.03	
q_e		3.3	3.3	3.0	2.8	2.7	2.4	2.2	2.0	1.7	1.2	0.8	0.4	
%removal		66.2	66.0	61.0	56.7	54.1	48.3	45.0	39.7	34.9	24.8	17.1	8.4	

Sr_s1	Sr-S1-st	Sr-S1-eq	Sr-S1-1	Sr-S1-2	Sr-S1-3	Sr-S1-4	Sr-S1-5	Sr-S1-6	Sr-S1-7	Sr-S1-8	Sr-S1-9	Sr-S1-10	Sr-S1-11	Sr-S1-12
Conc. [µg/L]	10000	180	205	223	242	269	288	327	344	371	405	497	611	849
pH		8.54	8.21	7.87	7.51	7.12	6.71	6.38	5.91	5.34	5.04	4.64	4.30	4.00
q_e		4.9	4.9	4.9	4.9	4.9	4.9	4.8	4.8	4.8	4.8	4.8	4.7	4.6
%removal		98.2	97.9	97.8	97.6	97.3	97.1	96.7	96.6	96.3	95.9	95.0	93.9	91.5

Sr_s2	Sr-S2-st	Sr-S2-eq	Sr-S2-1	Sr-S2-2	Sr-S2-3	Sr-S2-4	Sr-S2-5	Sr-S2-6	Sr-S2-7	Sr-S2-8	Sr-S2-9	Sr-S2-10	Sr-S2-11	
Conc. [µg/L]	10000	2032	2276	2432	2547	2764	2875	3022	3253	3623	4012	4436	5232	
pH		8.53	8.2	7.795	7.424	6.901	6.525	5.981	5.48	5.115	4.654	4.37	4.082	
q_e		4.0	3.9	3.8	3.7	3.6	3.6	3.5	3.4	3.2	3.0	2.8	2.4	
%removal		79.7	77.2	75.7	74.5	72.4	71.3	69.8	67.5	63.8	59.9	55.6	47.7	

Zn_n	Zn-n-st	Zn-n-eq	Zn-n-1	Zn-n-2	Zn-n-3	Zn-n-4	Zn-n-5	Zn-n-6	Zn-n-7	Zn-n-8	Zn-n-9	Zn-n-10	Zn-n-11	
Conc. [µg/L]	9938	587	636	950	2672	4201	5425	6221	7261	7448	7753	8132	8617	
pH		8.44	8.10	7.75	7.40	6.96	6.55	6.10	5.50	5.09	4.66	4.30	4.01	
q_e		4.7	4.7	4.5	3.6	2.9	2.3	1.9	1.3	1.2	1.1	0.9	0.7	
%removal		94.1	93.6	90.4	73.1	57.7	45.4	37.4	26.9	25.1	22.0	18.2	13.3	

Zn_s1	Zn-s1-st	Zn-s1-eq	Zn-s1-1	Zn-s1-2	Zn-s1-3	Zn-s1-4	Zn-s1-5	Zn-s1-6	Zn-s1-7	Zn-s1-8	Zn-s1-9	Zn-s1-10	Zn-s1-11	
Conc. [µg/L]	10009	28	25	19	40	45	41	49	161	915	1193	1904	2791	
pH	5.89	8.43	8.10	7.69	7.25	6.84	6.40	6.10	5.72	5.30	4.85	4.40	4.01	
q_e		5.0	5.0	5.0	5.0	5.0	5.0	5.0	4.9	4.5	4.4	4.1	3.6	
%removal		99.7	99.8	99.8	99.6	99.5	99.6	99.5	98.4	90.9	88.1	81.0	72.1	

Zn_s2	Zn-s2-st	Zn-s2-eq	Zn-s2-1	Zn-s2-2	Zn-s2-3	Zn-s2-4	Zn-s2-5	Zn-s2-6	Zn-s2-7	Zn-s2-8	Zn-s2-9	Zn-s2-10	Zn-s2-11	
Conc. [µg/L]	10004	155	196	411	733	1028	1303	1406	1604	1900	2680	3059	3570	
pH		8.455	8.09	7.699	7.235	6.88	6.45	6.149	5.713	5.172	4.754	4.363	4.021	
q_e		4.9	4.9	4.8	4.6	4.5	4.4	4.3	4.2	4.1	3.7	3.5	3.2	
%removal		98.4	98.0	95.9	92.7	89.7	87.0	85.9	84.0	81.0	73.2	69.4	64.3	